Topologic and Geometric Approaches for In Vivo Quantitative Assessment of Trabecular Bone Micro-Architecture

Punam Kumar Saha
Professor
Departments of ECE and Radiology
University of Iowa
pksaha@engineering.uiowa.edu

Overview

- Osteoporosis
- Osteoporosis Imaging
- Trabecular Plate Rod Microarchitecture
- Bone Measures using Multi-row Detector CT Imaging
- Results from Human Studies

Overview

- Osteoporosis
- Osteoporosis Imaging
- Trabecular Plate Rod Microarchitecture
- Bone Measures using Multi-row Detector CT Imaging
- Results from Human Studies

Osteoporosis

- The word osteoporosis literally means “porous bones”
- Over time, osteoporosis reduces bone mass and degenerates bone structure, and therefore bone strength is decreased
- Thus, bone becomes fragile and easy to break
- For someone with severe osteoporosis, even a sudden movement may cause bone fracture

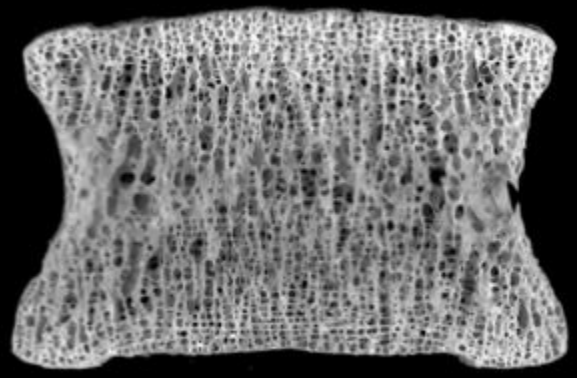

Normal bone in vertebrae

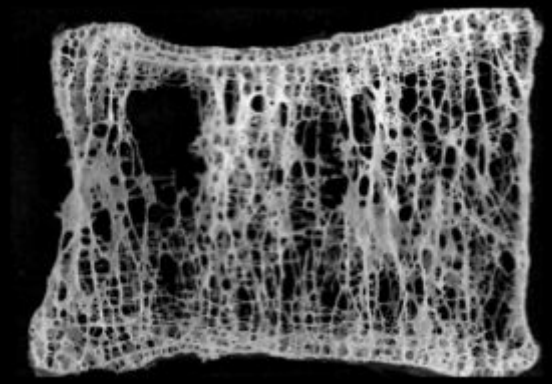

Same bone location in a osteoporosis patient

http://www.bonedisease.info/disease/osteoporosis/which-bone-affected-by-osteoporosis-the-most/

Osteoporosis and Fractures

- Osteoporosis affects nearly half of the men and women over the age of 75
- About 44 million people in the United States are at risk for osteoporosis causing 1.5 million fragility fractures annually
- Nearly, 40% of women and 13% of men suffer a fragility fracture in their lifetimes
- The estimated number of hip fractures worldwide will rise from 1.66 million in 1990 to 6.26 million in 2050
- Major osteoporosis fractures occur at hip, spine and forearm
- Osteoporotic hip fractures are especially devastating, reducing life expectancy by 10-20%
- More than three-quarters of all hip fractures occur in women

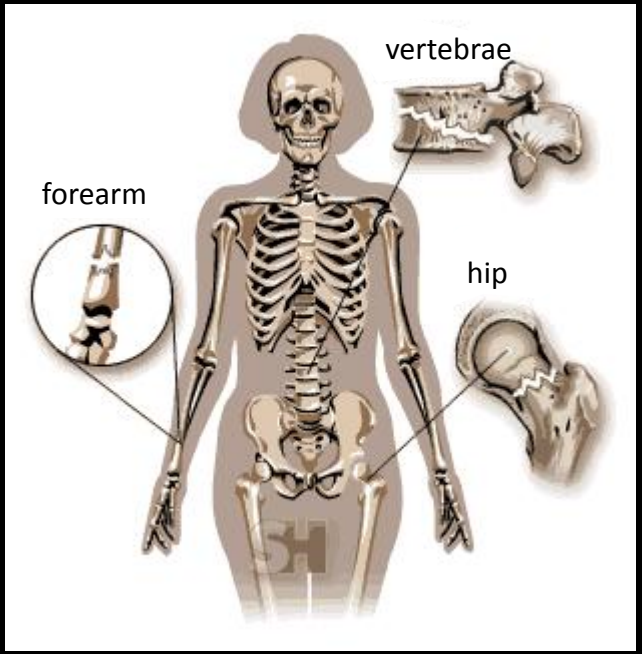

Major fracture sites

http://www.vidasaludynegocios.com/index.php?dispatch=products.view&product_id=30529

Treatments

- Treatment includes medication, healthy diet, and weight-bearing exercise to help prevent bone loss and strengthen already weak bones
- Self-care
  - ✓ Healthy diet
  - ✓ Physical exercise
  - ✓ Stop smoking
- Medications
  - ✓ Vitamin
  - ✓ Dietary supplement
  - ✓ Antacid
  - ✓ Bone health
  - ✓ Hormone

Treatments

- Treatment includes medication, healthy diet, and weight-bearing exercise to help prevent bone loss and strengthen already weak bones
- Self-care
  - ✓ Healthy diet
  - ✓ Physical exercise
  - ✓ Stop smoking
- Medications
  - ✓ Vitamin
  - ✓ Dietary supplement
  - ✓ Antacid
  - ✓ Bone health
  - ✓ Hormone

- Therapeutic treatments for osteoporosis are expensive with associated side effects
- Accurate assessment of fracture risk, and clear guidelines to initiate preventive interventions and monitor treatment response, are urgent needs in public health
- **Osteoporotic imaging** plays a central role in that process

Overview

- Osteoporosis
- Osteoporosis Imaging
- Trabecular Plate Rod Microarchitecture
- Bone Measures using Multi-row Detector CT Imaging
- Results from Human Studies

Dual-Energy X-Ray Absorptiometry (DXA)

- At present, dual-energy X-ray absorptiometry (DXA) measured areal BMD is used to diagnose osteoporosis
- DXA measures of whole body, hip and spine are popularly used
- Being an areal 2-D measure, DXA has several limitations
  - ✓ sensitivity to bone size, thus overestimating fracture risk in individuals with small body size
  - ✓ lack of accuracy in the setting of degenerative changes in the hip and spine
- It is known that the majority of individuals who suffer fragility fractures are misclassified by DXA as not having osteoporosis, i.e., their T-scores are actually > -2.5

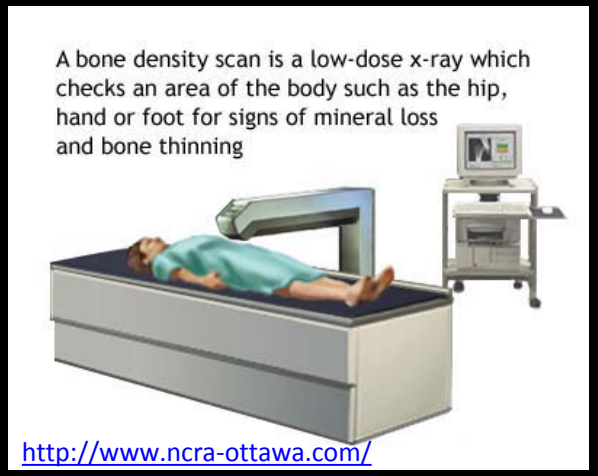

http://www.ncra-ottawa.com/

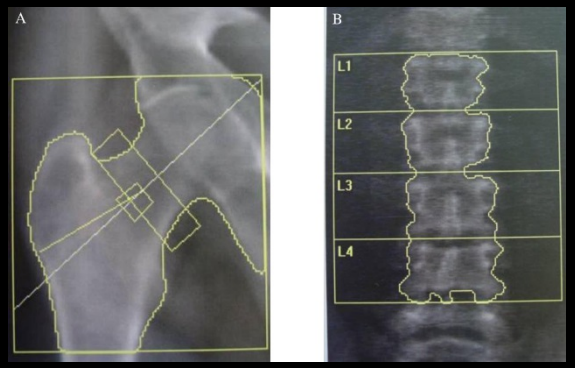

DEXA assessment of BMD of the femoral neck (A) and the lumbar spine (B)
https://en.wikipedia.org/wiki/Dual-energy_X-ray_absorptiometry

Osteoporosis and Bone Structure

There are two types of bone

- Cortical bone (Cb) is the hard outer layer of the bone
- Trabecular bone (Tb) is the sponge-like internal structure of the bone
- Cb is denser, stronger, and stiffer for more strenuous activities
- Cb can sustain greater stress but less strain before failure
- Tb can sustain larger strains before failing
- Tb has a greater capacity to store energy since it is porous and filled with fluid
- Osteoporosis can lead to thinning of both types of bone which makes bones more susceptible to breaks

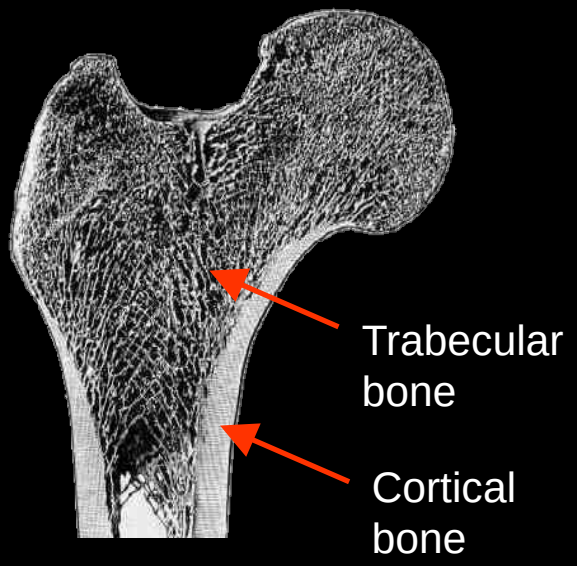

Bone Mineral Density and Mechanics

How Predictive is bone mineral density (BMD) of the Bone's Mechanical Behavior?

- Meta analysis
- N=38 (1985-2000)
- Various parameters of "strength"
- Mean r^2 = 0.64±0.17

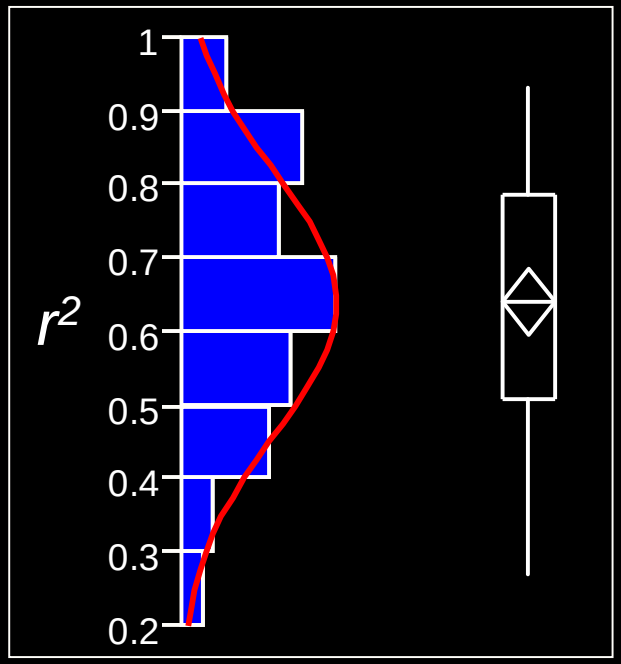

BMD only accounts for approximately 60 to 70% of the variability in bone strength

Bone Mineral Density and Structure

- Although osteoporosis is defined by low BMD, BMD explains 60-70% of the variability in bone strength
- The remaining variability due to the cumulative and synergistic effects of other factors, including geometry and micro-architecture of Cb and Tb
- Several clinical studies have reported that cortical bone thinning and high porosity is associated with increased risk of osteoporotic low-trauma fractures
- A large number of histologic studies have confirmed the relationship between erosion of trabeculae from plates to rods and fracture risk
- Reduced trabecular connectivity are observed in patients with vertebral crush fractures
- There is evidence suggesting that reduced transverse trabeculae are associated with decreased bone strength leading to failure due to buckling of longitudinal trabeculae

Normal

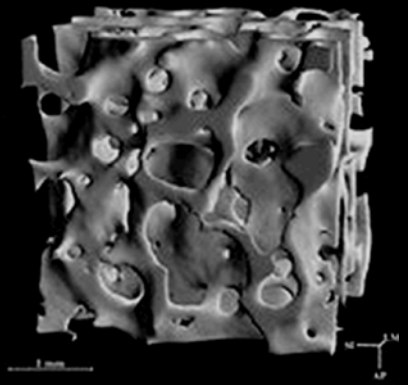

Osteoporosis

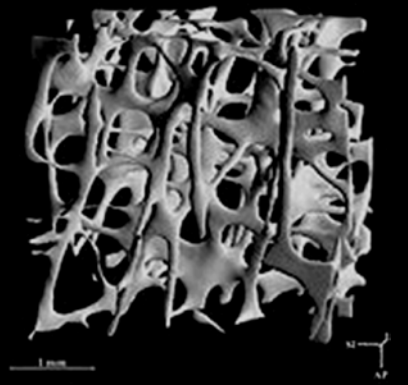

Hildebrand et al, JBMR, 1999

Bone Biopsy

Quantifying Architecture via Bone Biopsy

- Iliac crest or rib
- Painful, risky, and limited retests
- Not suitable for controls or time-series analysis

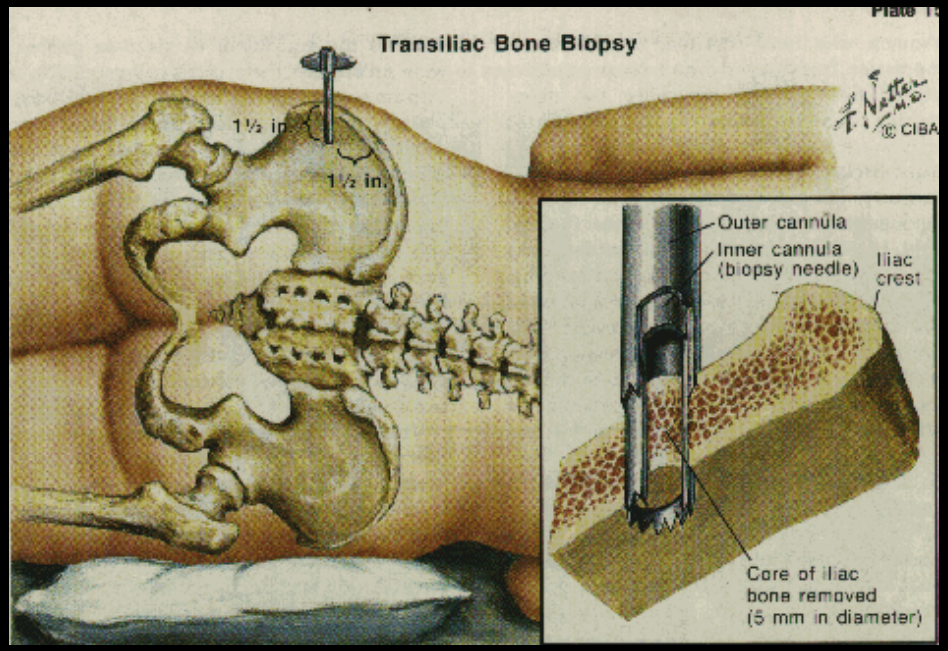

In Vivo Imaging Offers an Opportunity for Virtual Bone Biopsy

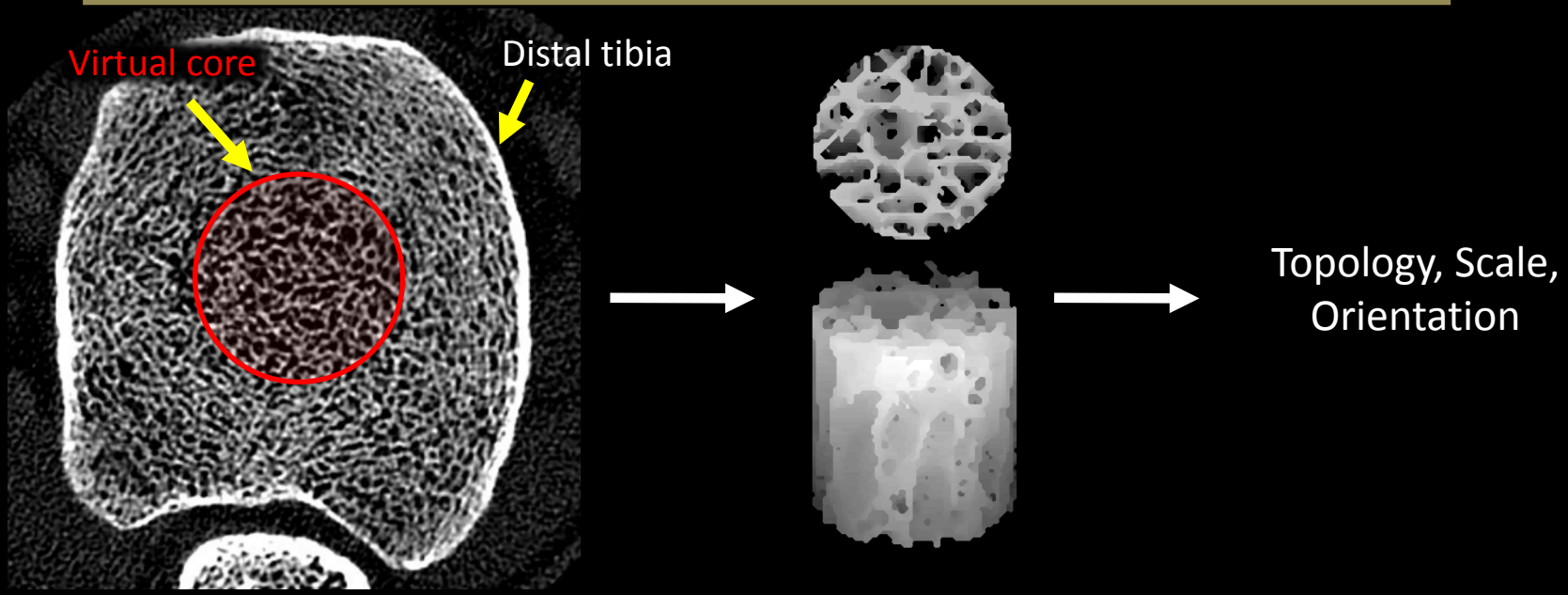

Features

- Analogous to bone biopsy
- Virtual core is isolated from 3D image data sets.
- Core is subjected to analysis

Challenges

- Reduced resolution
- Limited signal-to-noise ratio

Overview

- Osteoporosis
- Osteoporosis Imaging
- Trabecular Plate Rod Microarchitecture
- Bone Measures using Multi-row Detector CT Imaging
- Results from Human Studies

Topology of Trabecular Networks

Topological analysis of line skeletonized structure

3D Euler Poincaré Formula:

χ = objects - tunnels + cavities
= nodes - edges + faces

Connectivity Index = $1 - \chi$

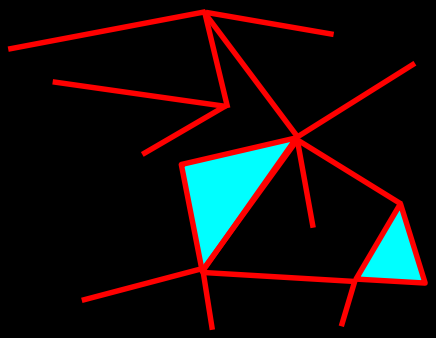

objects: 1
tunnels: 1
cavities: 0

nodes: 17
edges: 19
faces: 2

$\chi = 0$

Structure-Model Index (SMI)

SMI μ ($\partial S/\partial r$)

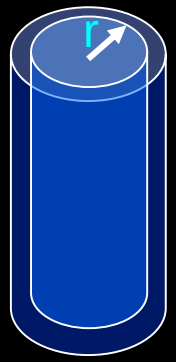

SMI=relative change in surface area (S) upon radial (r) expansion

calcaneus

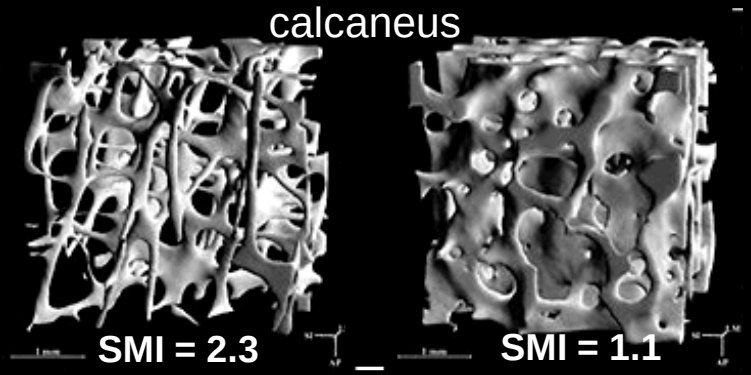

Hildebrand et al, J Bone Miner Res, 1999

Trabecular Plate-Rod Characterization using Digital Topological Analysis

- Topological class (curve, surface junctions) at any location may be unambiguously determined from the topological numbers (#objects (ξ), #tunnels (η), and #cavities (δ))
- Edge: $\xi = 1; \eta = 0; \delta = 0$
- Curve Interior: $\xi = 2; \eta = 0; \delta = 0$
- Surface Interior: $\xi = 1; \eta = 1; \delta = 0$
- Curve-Curve junction: $\xi > 2; \eta = 0; \delta = 0$
- Surface-Curve junction: $\xi > 1; \eta = 1; \delta = 0$
- Surface-Surface junction: $\xi = 1; \eta > 1; \delta = 0$

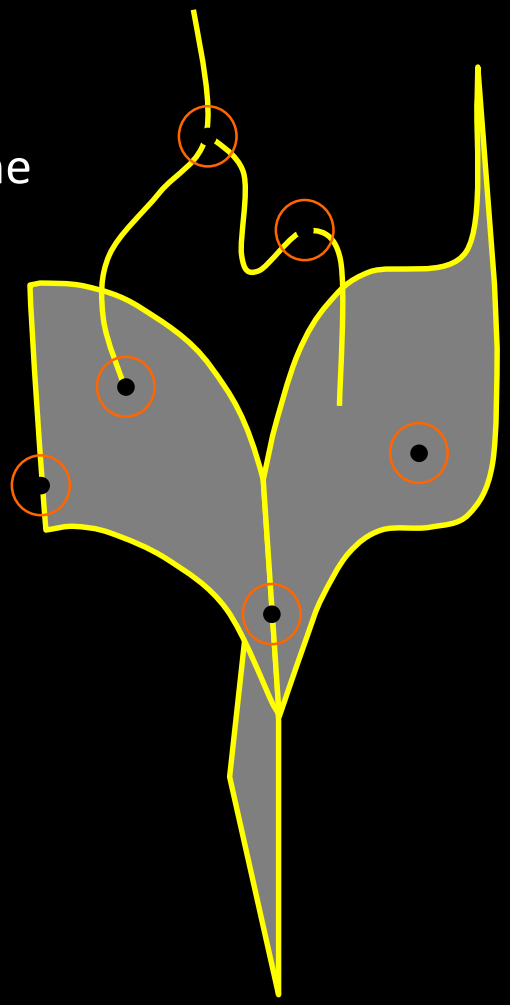

Digital Topological Analysis

- Identifies plates/rods and other topological entities
- Able to distinguish between fracture/ non-fracture groups via *in vivo* MRI
- Being used by several leading research groups

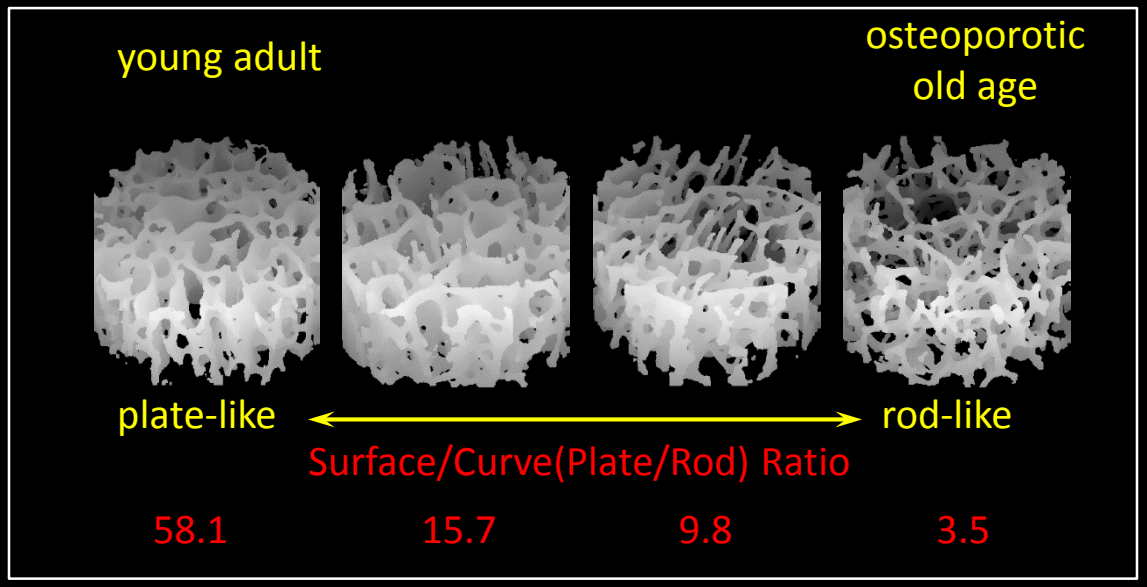

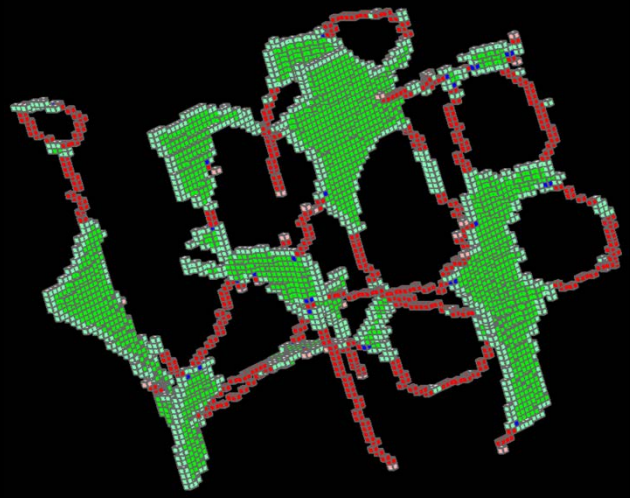

Surface = plate
Rod = curve
Junction

Age and disease-related topological changes

Volumetric Topological Analysis

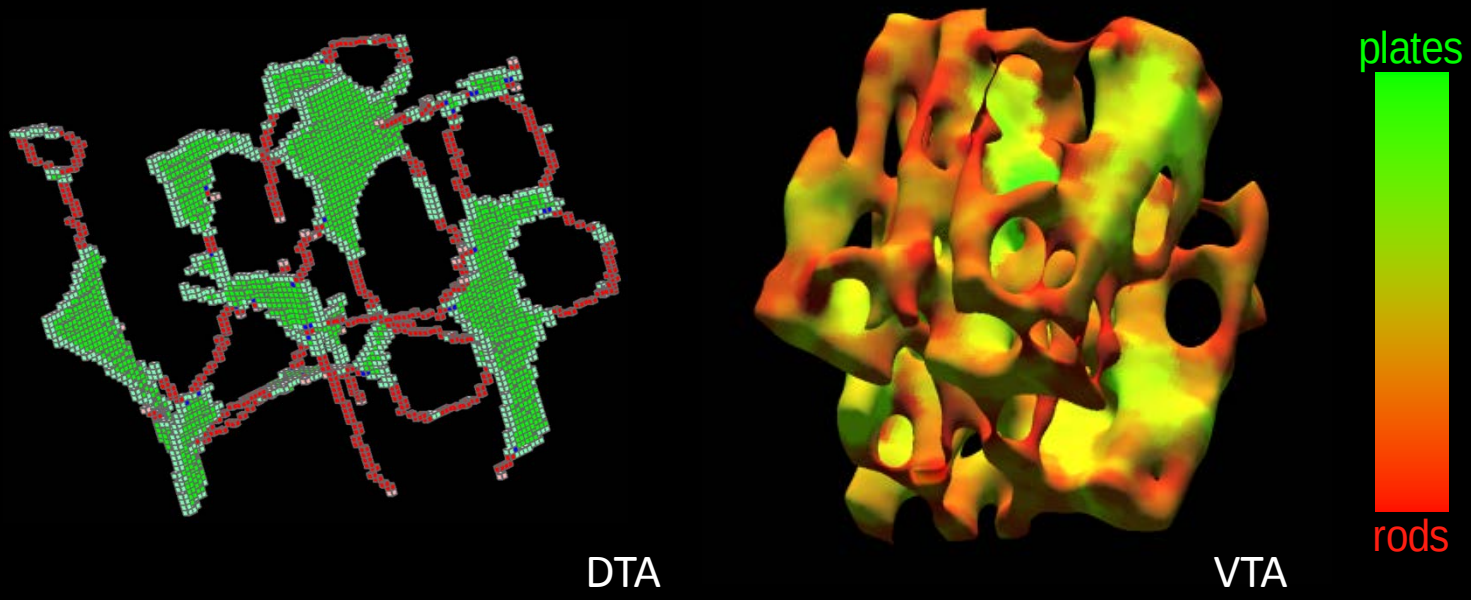

- Quantify trabecular bone architecture at *in vivo* resolution
  - Plateness and rodness on the continuum between perfect plates and perfect rods
  - More accurately captures gradual conversion from Tb plates to rods at the level of individual trabeculae

Tensor Scale Analysis

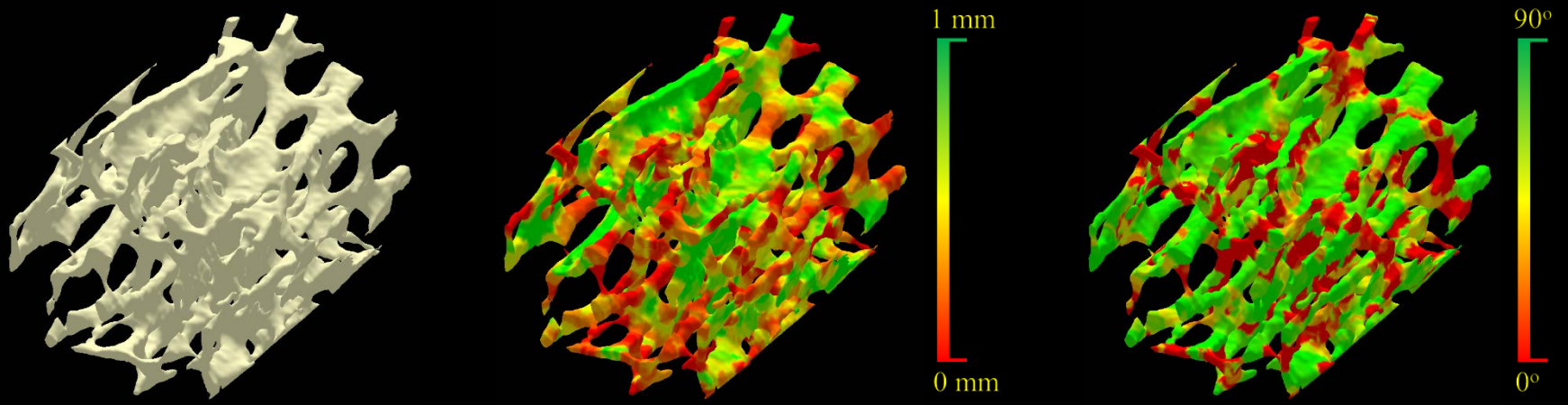

- Quantify trabecular bone architecture at *in vivo* resolution
  - Plateness and rodness on the continuum between perfect plates and perfect rods
  - Local trabecular orientation classifying longitudinal (vertical) and transverse (horizontal) structures

Trabecular Plate-Rod Measures and Bone Strengths

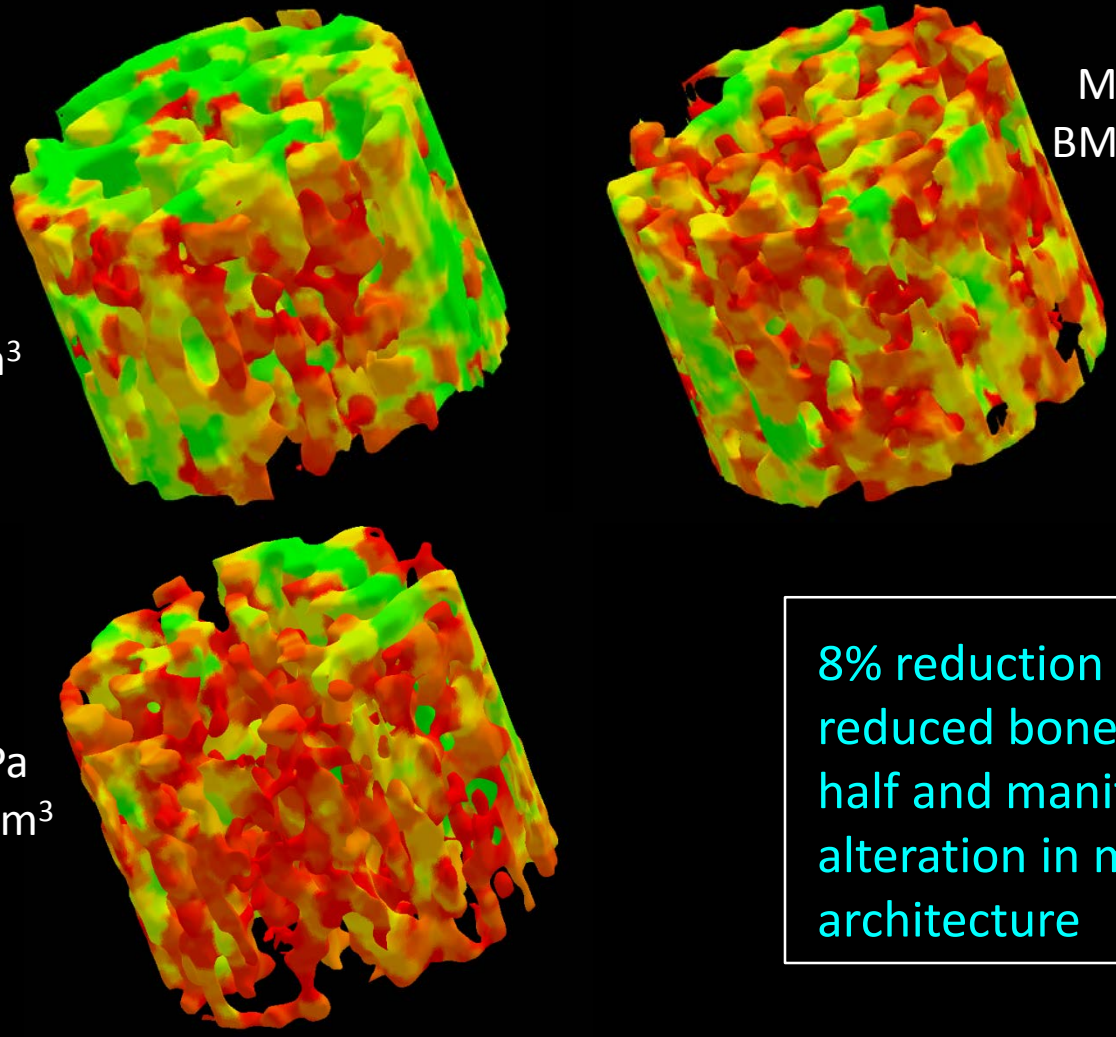

Modulus: 3.3 GPa
BMD: 1.31 gm/cm^3
Tb.PW : 464 µm
Tb.PR: 0.58

Modulus: 2.2 GPa
BMD: 1.27 gm/cm^3
Tb.PW: 385 µm
Tb.PR: 0.38

Modulus: 1.5 GPa
BMD: 1.20 gm/cm^3
Tb.PW: 340 µm
Tb.PR: 0.26

8% reduction in BMD reduced bone strength to half and manifest a 50% alteration in micro-architecture

Ability To Predict Mechanical Properties

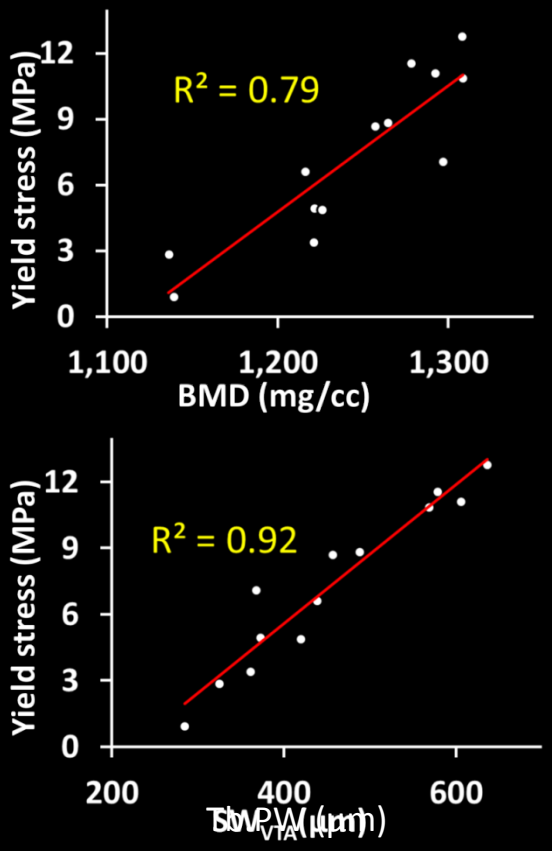

High predictability of experimental biomechanical properties.

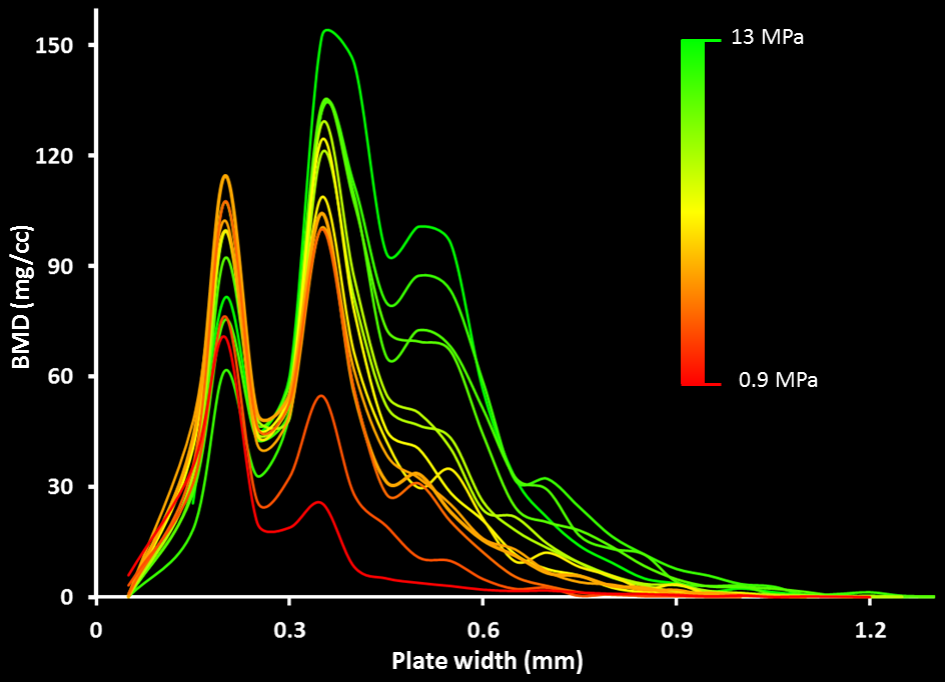

Bone mass distribution at different plate width: a new class of information

Bone Micro-Architecture among Eugonadal and Hypogonadal Men

N = 20 MRI Study (age and race-matched)

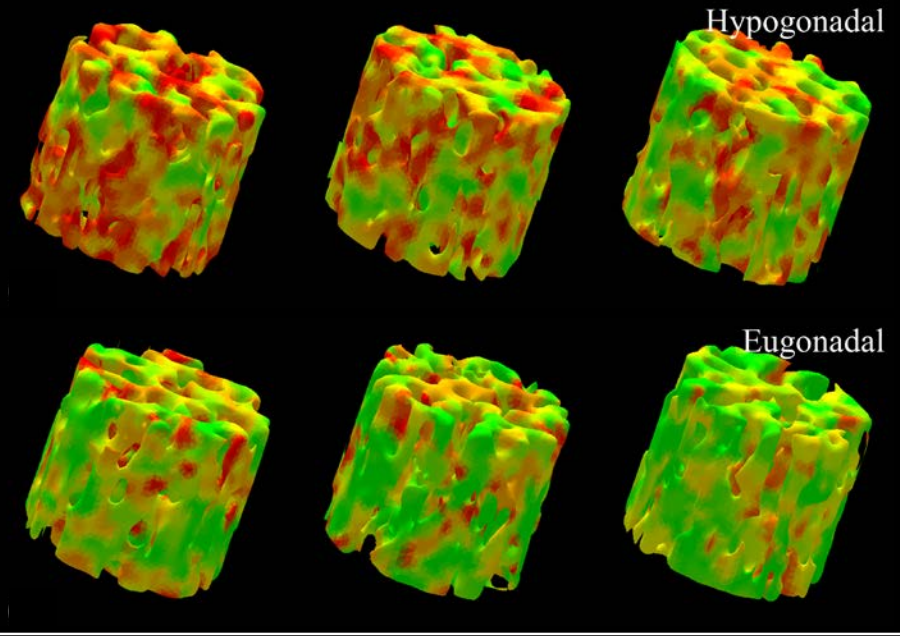

Trabecular bone plate-rod micro-architecture among hypogonadal and eugonadal men

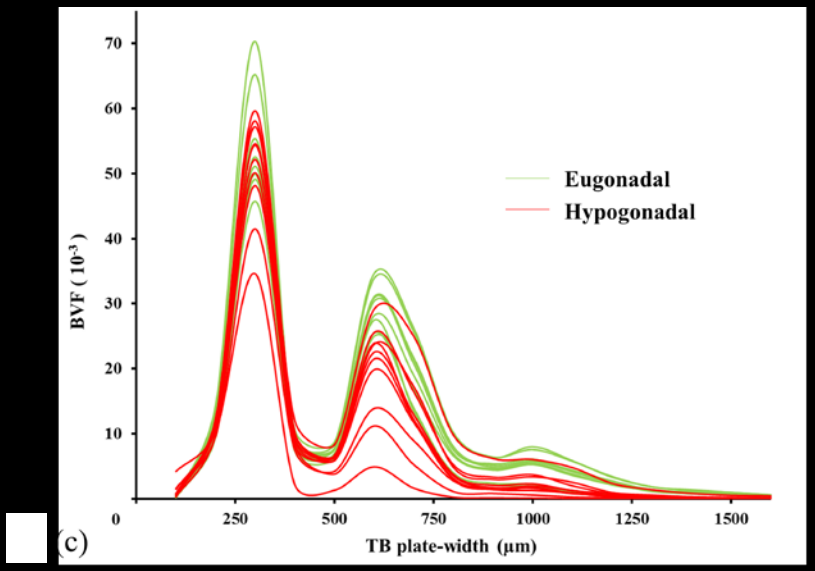

Bone mass distribution at different plate width: a new class of information

- 44 % (p = 0.001) greater Tb plates in eugonadal men than hypogonadal men
- No significant difference in rod volume

Treatment Effects Hypogonadal Men

N = 10 Two year follow-up MRI study

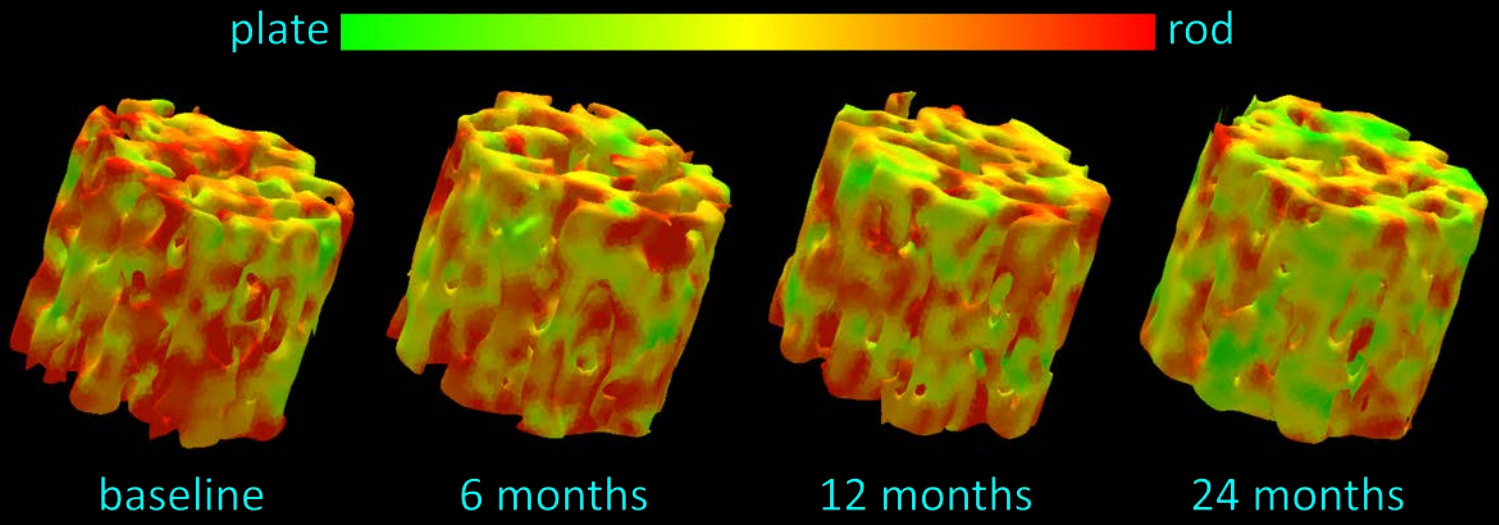

Treatment effects in trabecular bone plate-rod micro-architecture in hypogonadal men

- 6.5 % (p = 0.06) increase in trabecular bone plate volume after 6 months
- 16.2 % (p = 0.003) increase in trabecular bone plate volume after 24 months
- No significant difference in rod volume even after 24 months of treatment

Overview

- Osteoporosis
- Osteoporosis Imaging
- Trabecular Plate Rod Microarchitecture
- Bone Measures using Multi-row Detector CT Imaging
- Results from Human Studies

Major Advantages of Modern MDCT Scanners

- High spatial resolution: State-of-the-art CT scanners provide high spatial resolution allowing segmentation and quantitative assessment of TB micro-architecture
  - ✓ The Siemens Force scanner achieves 167 µm (10% MTF) in-plane resolution and 282 µm (10% MTF) z-plane resolution
- Ultra-high speed scanning: Modern CT scanners are capable of acquiring a 10 cm scan-length at a peripheral site using an UHR mode in just 6.8 sec
- Ultra-low radiation: Modern MDCT scanners allow high resolution Tb imaging at less than 50 µSv radiation dose
- Large scan-length: Useful for automatic selection of anatomically consistent regions-of-interest (ROIs)
  - ✓ Positioning error is a serious challenge for HR-pQCT
  - ✓ A positioning error by 0.5 mm may result in a 2% error in bone measures at the distal tibia

MDCT Scan Protocol

- Single X-ray source spiral acquisition at 120 kV, 100 effective mAs, 1sec rotation speed, pitch factor: 1.0
- Number of detector rows: 64
- Scan time: 5.8 seconds, collimation: 64× 0.6 mm
- Total effective dose equivalent: 50 µSv ≈ 5 days of environmental radiation in the United States
- Siemens z-UHR scan mode is applied enabling Siemens double z sampling technology
- Images are reconstructed at 400 µm slice-thickness with 200 µm slice-spacing and 150 µm pixel-size using Siemens's special kernel Ur77u with Edge Technology to achieve high spatial resolution

In Vivo MDCT Scan Setup

- Laser beam projections are used to align the tibial long axis with the central z axis of the scanner
- This alignment step is important to achieve the highest image resolution and to standardize trabecular bone measures
- The distal tibial end-plateau is included in the FOV used as reference to determine different tibial locations for ROI selection

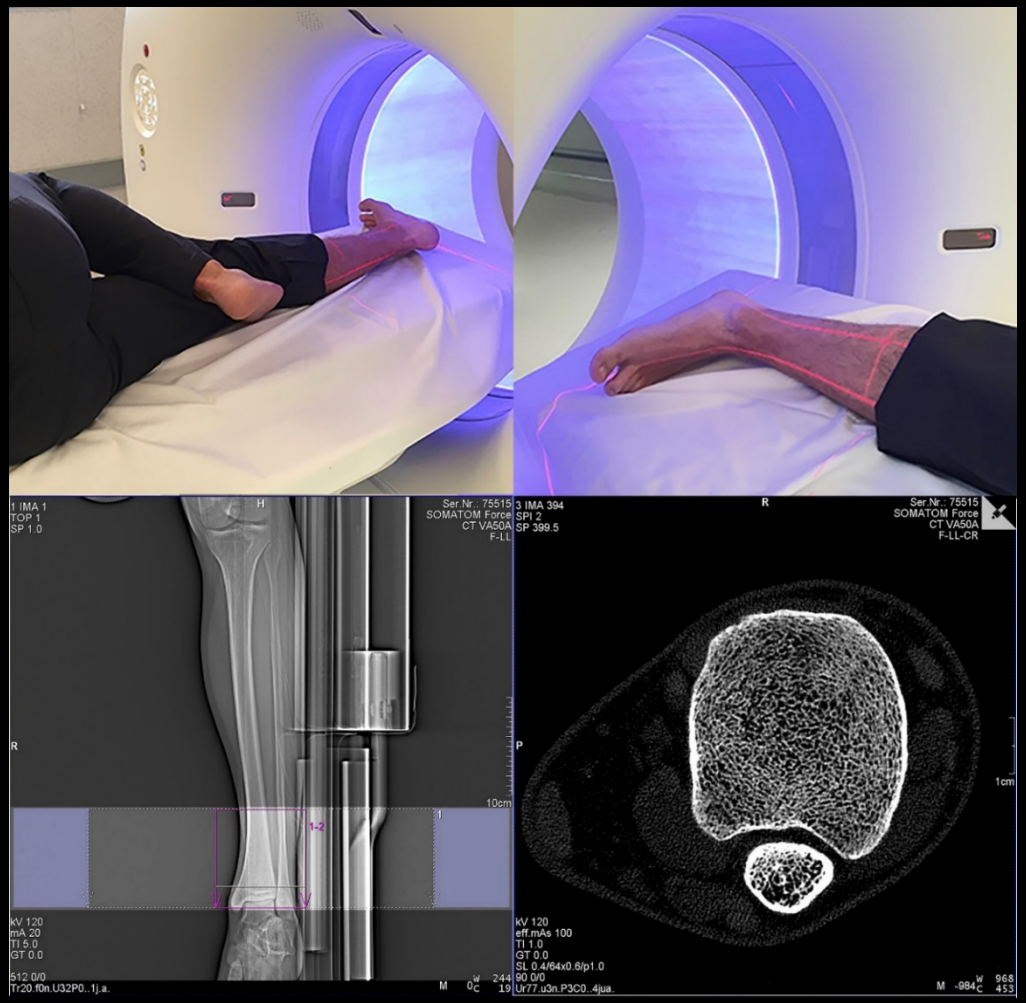

The List of MDCT Derived Tb Measures

Parameter (unit)	*Description*
vBMD (mg/cm^3)	Volumetric trabecular bone mineral density
tBMD (mg/cm^3)	Volumetric trabecular bone mineral density contributed by transverse trabeculae characterized by tensor scale analysis
Tb.NA (cm^2/cm^3)	Trabecular bone network area density, i.e., the average area of the medial surface of segmented bone per unit VOI
Tb.PW (μm)	Mean trabecular plate-width computed by tensor scale analysis
Tb.PR (no unit)	Ratio of total plateness and rodness counts over a VOI computed by tensor scale analysis
Tb.Th (μm)	Mean trabecular thickness computed by star-line analysis
Tb.Sp (μm)	Mean trabecular separation, i.e., the space between trabecular structures computed by star-line analysis
EI (no unit)	Erosion index—a summary measure of digital topological analysis of TB aimed to represent the extent of bone erosion
SMI (no unit)	An indicator of the structure of trabeculae; SMI is '0' for parallel plates and '3' for cylindrical rods

Repeatability of MDCT Tb Measures

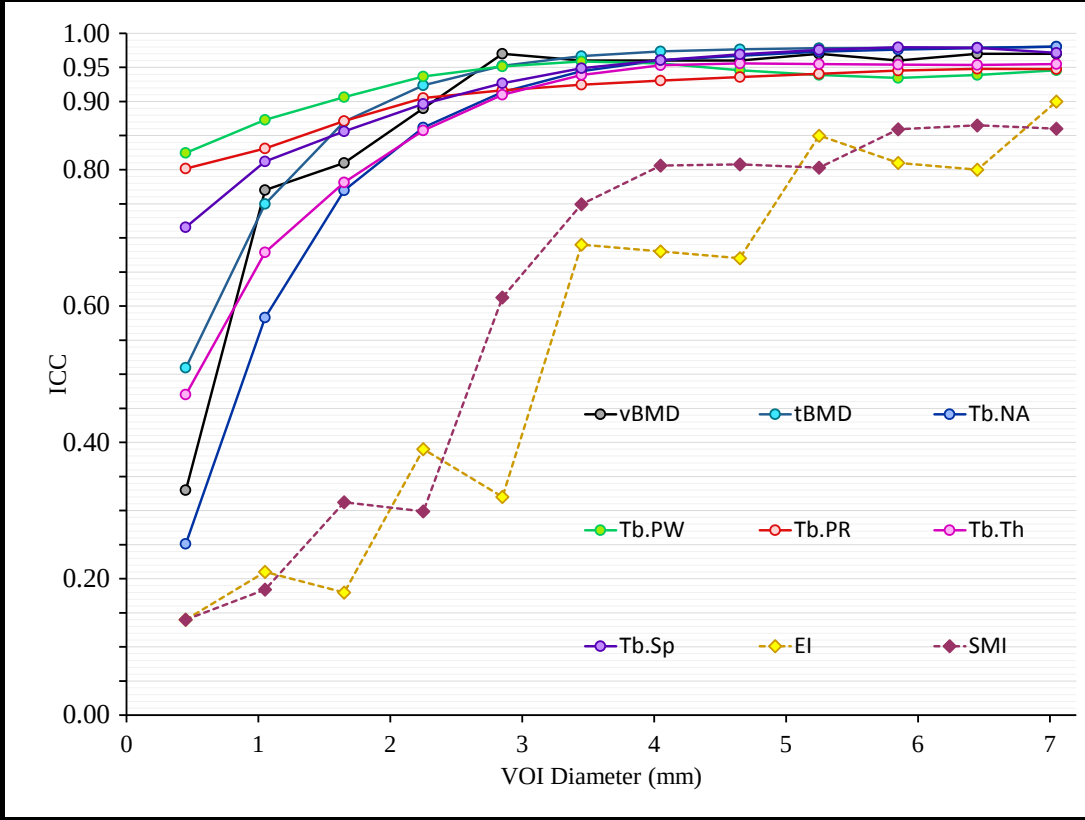

Repeat scan reproducibility of Tb measures on an MDCT scanner using cadaveric ankle specimens (n = 25)

Validation of MDCT Tb Measures

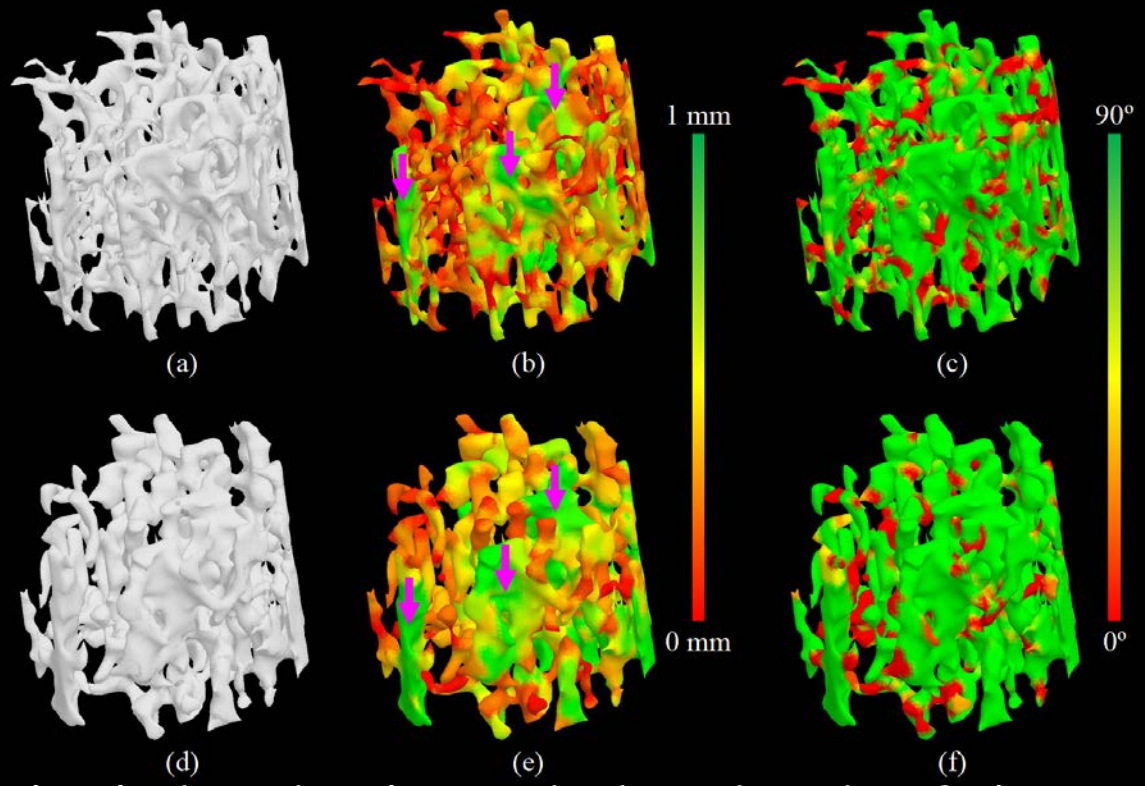

- Tb plate-rod and orientation characterization using micro-CT (top row) and MDCT scanners (bottom row)
- Although, the effects of resolution difference between the two scanners are apparent, regional agreement of microstructural characterization is notable

Validation of MDCT Tb Measures

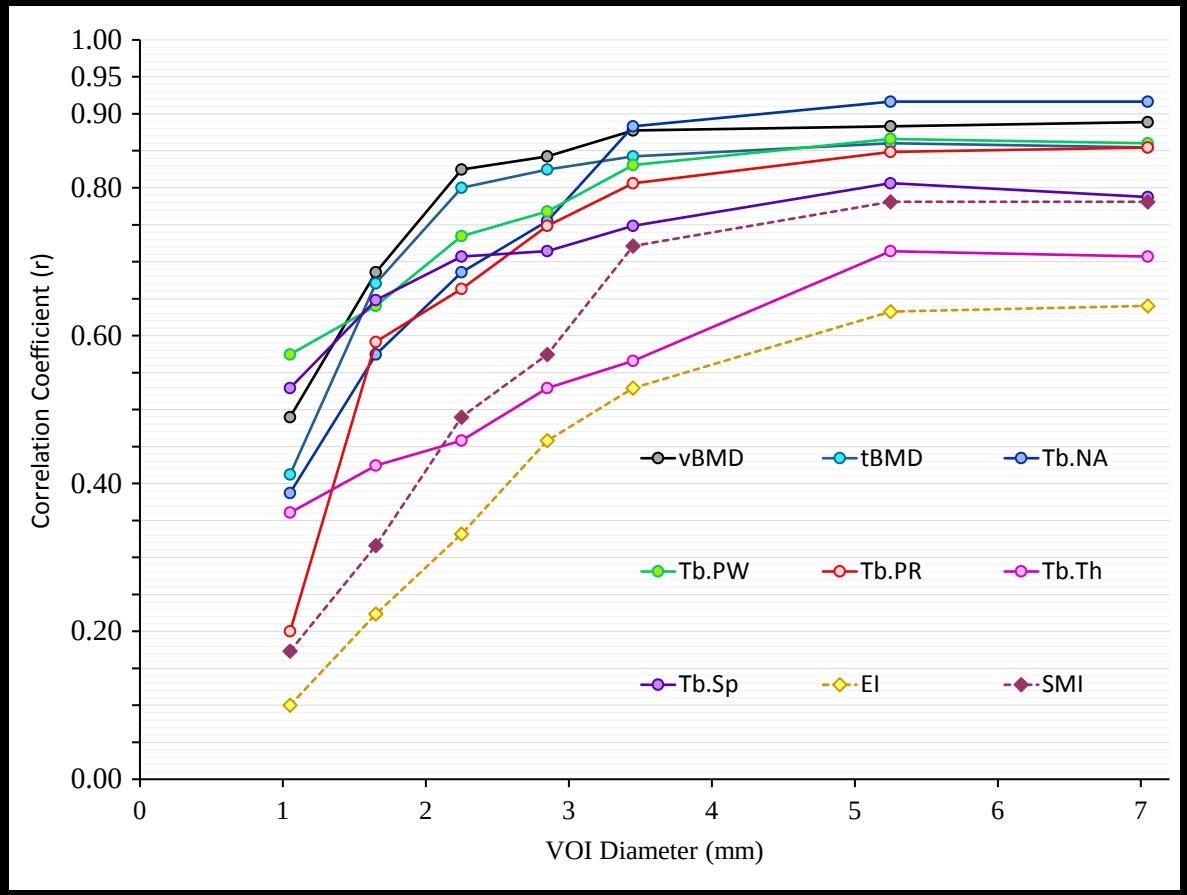

Correlation analysis of the values of Tb measures derived from micro-CT and MDCT imaging of cadaveric ankle specimens (n = 25)

Validation of MDCT Tb Measures

TB measure	Correlation Coefficients (r)	micro-CT (mean value)	MDCT (mean value)
vBMD (mg/cm^3)	0.88	1158	993
tBMD (mg/cm^3)	0.86	194	120
Tb.NA (cm^2/cm^3)	0.92	0.10	0.07
Tb.PW (µm)	0.87	541	861
Tb.PR (no unit)	0.85	2.85	7.02
Tb.Th (µm)	0.71	133	160
Tb.Sp (µm)	0.81	348	468
EI (no unit)	0.63	0.20	0.67
SMI (no unit)	0.78	0.76	2.23

Correlation and mean values of Tb measures derived from micro-CT and MDCT imaging of cadaveric ankle specimens at VOI size of 5.25 mm (n = 25)

Ability of MDCT Tb Measures to Predict Mechanical Properties

Measuring Elastic Properties

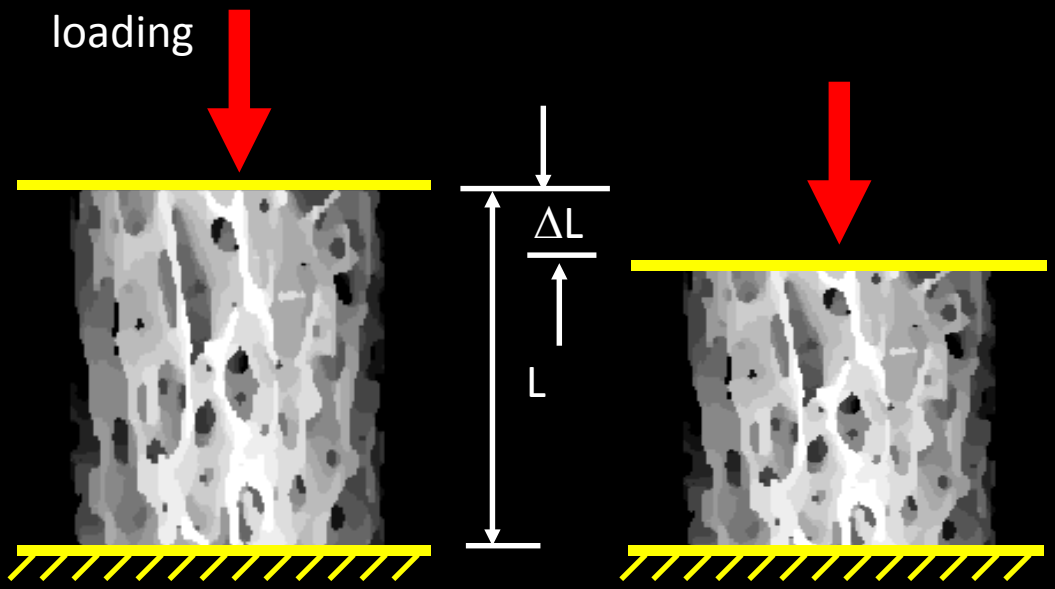

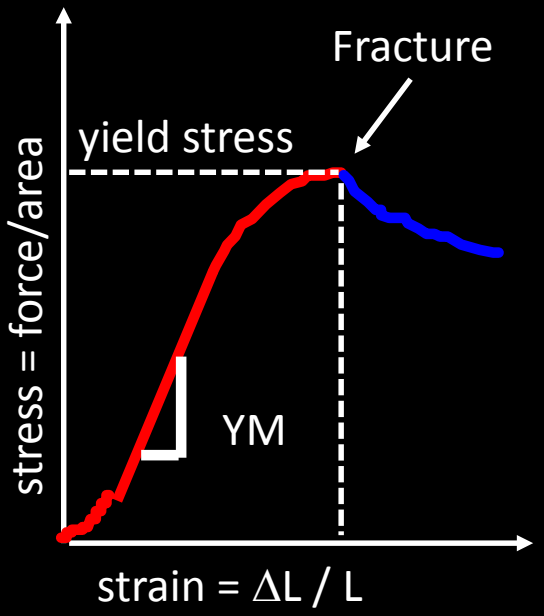

Young's Modulus (YM) = slope

Strains were recorded using an extensometer reading

Ability of MDCT Tb Measures to Predict Mechanical Properties

	Pearson correlation coefficient (r)			
	MDCT bone measures versus bone strength		micro-CT bone measures versus bone strength	
TB measure	Yield stress	Young's modulus	Yield stress	Young's modulus
vBMD (mg/cm^3)	0.785	0.698	0.763	0.738
tBMD (mg/cm^3)	0.861	0.813	0.872	0.791
Tb.NA (cm^2/cm^3)	0.855	0.712	0.838	0.807
Tb.PW (µm)	0.893	0.757	0.902	0.802
Tb.PR (no unit)	0.838	0.722	0.854	0.820
Tb.Th (µm)	0.849	0.765	0.817	0.685
Tb.Sp (µm)	0.851	0.730	0.848	0.764
EI (no unit)	0.780	0.536	0.781	0.670
SMI (no unit)	0.786	0.541	0.821	0.743

Correlation of different MDCT and micro-CT TB measures with yield stress and Young's modulus of TB cores from cadaveric ankle specimens determined by mechanical testing (n = 25)

Overview

- Osteoporosis
- Osteoporosis Imaging
- Trabecular Plate Rod Microarchitecture
- Bone Measures using Multi-row Detector CT Imaging
- Results from Human Studies

Study 1

Aim: To determine whether MDCT bone data from multiple scanners can be used in large multi-site or longitudinal studies

Data-Continuity for Tb Measures from Two MDCT Scanners (n = 20)

- A pertinent challenge with MDCT for bone research emerges due to wide variation in imaging and reconstruction features from different vendors and rapid upgrades in technology
- This raises concerns of data uniformity in large-scale multi-site or longitudinal studies that typically involve data from multiple scanners
- the distal tibia of twenty volunteers (age: 26.2 ± 4.5 Y, 10 female) was scanned using the Siemens SOMATOM Definition Flash and the higher resolution Siemens SOMATOM Force scanners with an average 45-day time gap between scans.

			10% MTF (lp/cm)	
Scanner	Kernel	CT parameters	xy-plane	z-direction
Siemens Flash	U70u	120 kV, 200mAs, pitch : 1	16.2	17.9
Siemens Force	Ur77u	120 kV, 100 mAs, pitch : 1	24.8	21.0

Resolution Effects for Two MDCT Scanners

MDCT images of the lower portion of the left leg of a healthy volunteer scanned using the Siemens Flash (low resolution) (upper row) and Force (high resolution) (lower row) scanners

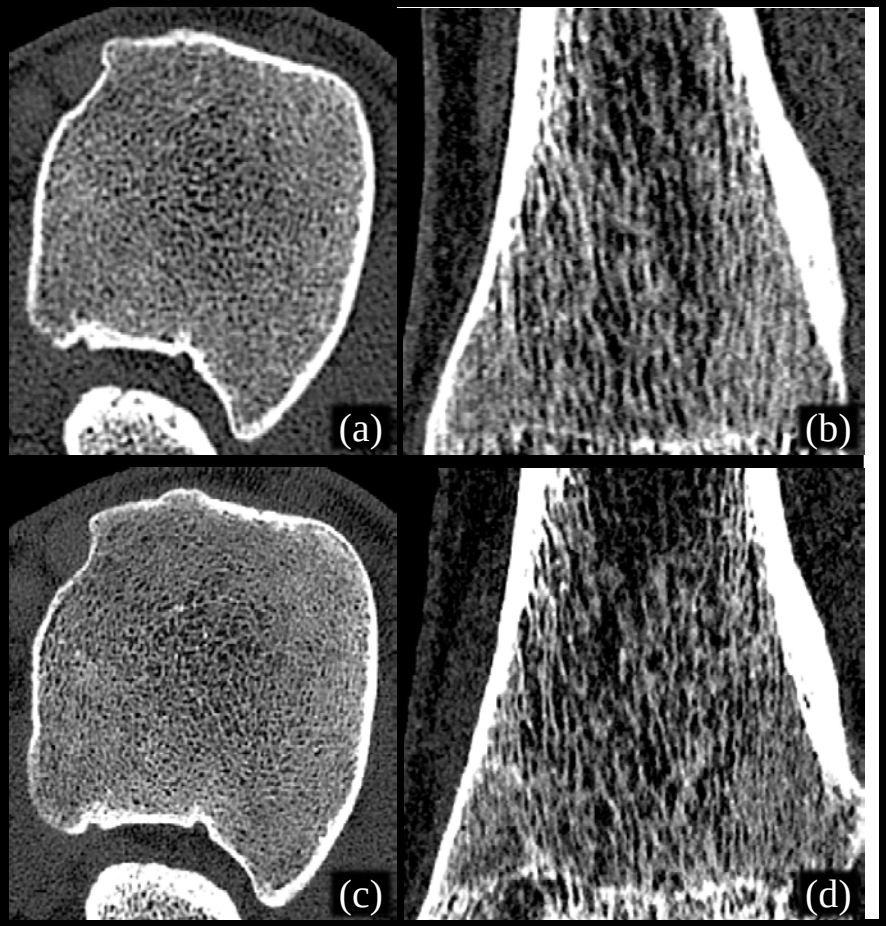

Correlation for Tb measures obtained from the Two Siemens Flash scanners

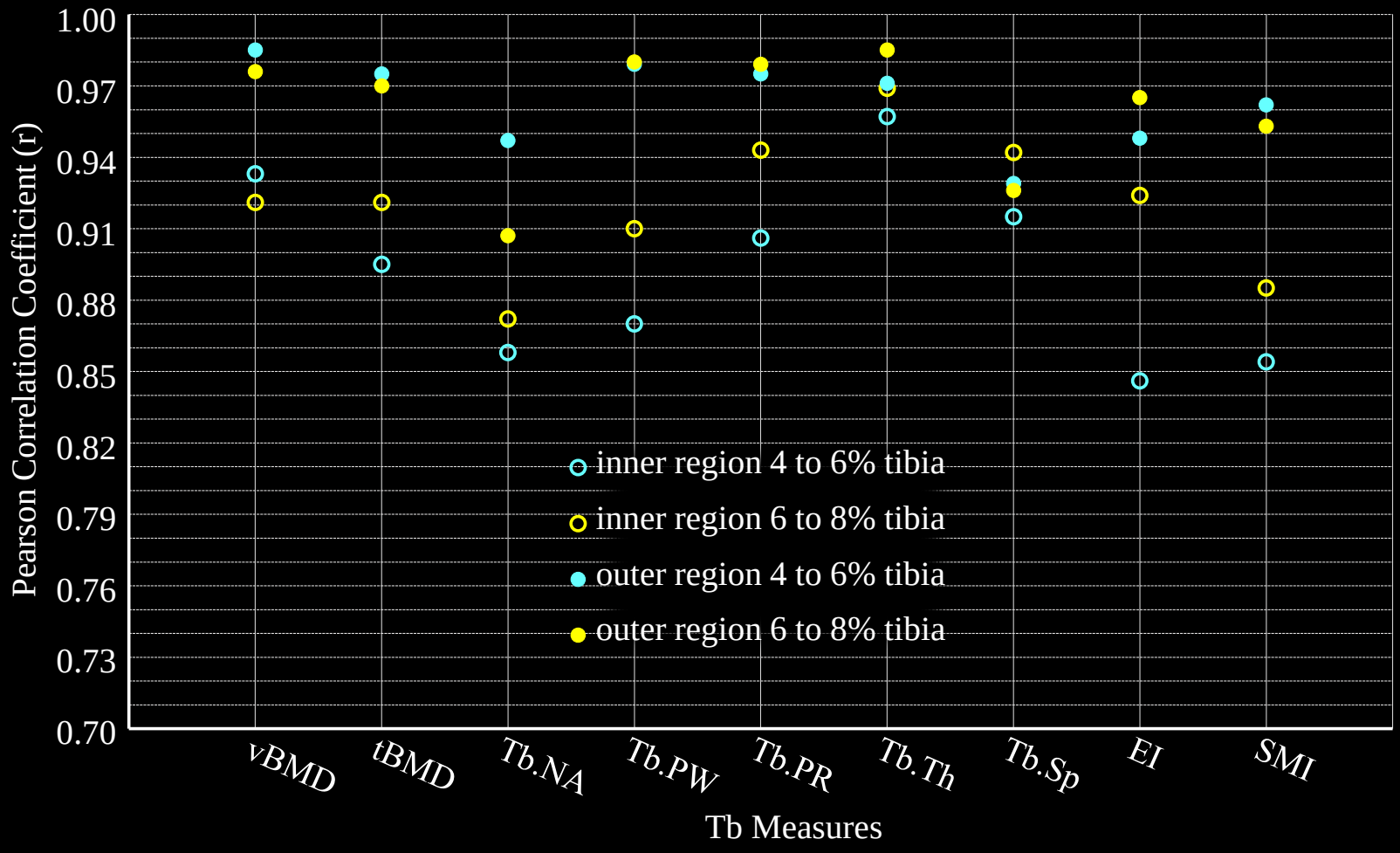

Discussion

- Tb micro-architectural measures estimated from the two different MDCT scanners possess high linear correlation ($r > 0.9$)
- Higher correlations of Tb measures from the two scanners were observed for the outer region at both the 4-6 % and 6-8% distal tibia
- *In vivo* measures of TB micro-architecture from two scanners can be used in a cross-sectional or longitudinal study after adjustments using calibration equations, if needed The calibration equations will be useful in multi-center studies to distinguish whether an observed difference in a parameter is associated with scanner differences or “real” difference between measured bones
- A non-significant interaction effect for distal tibial location of TB measures and slope showed that, for a TB measure, similar calibration is required independently of the location used for measurement
- All measures with lower CCCs would require some kind of calibration.

Study 2

Aim: To determine differences in bone structures in different human study groups

Results of a Human Pilot Study

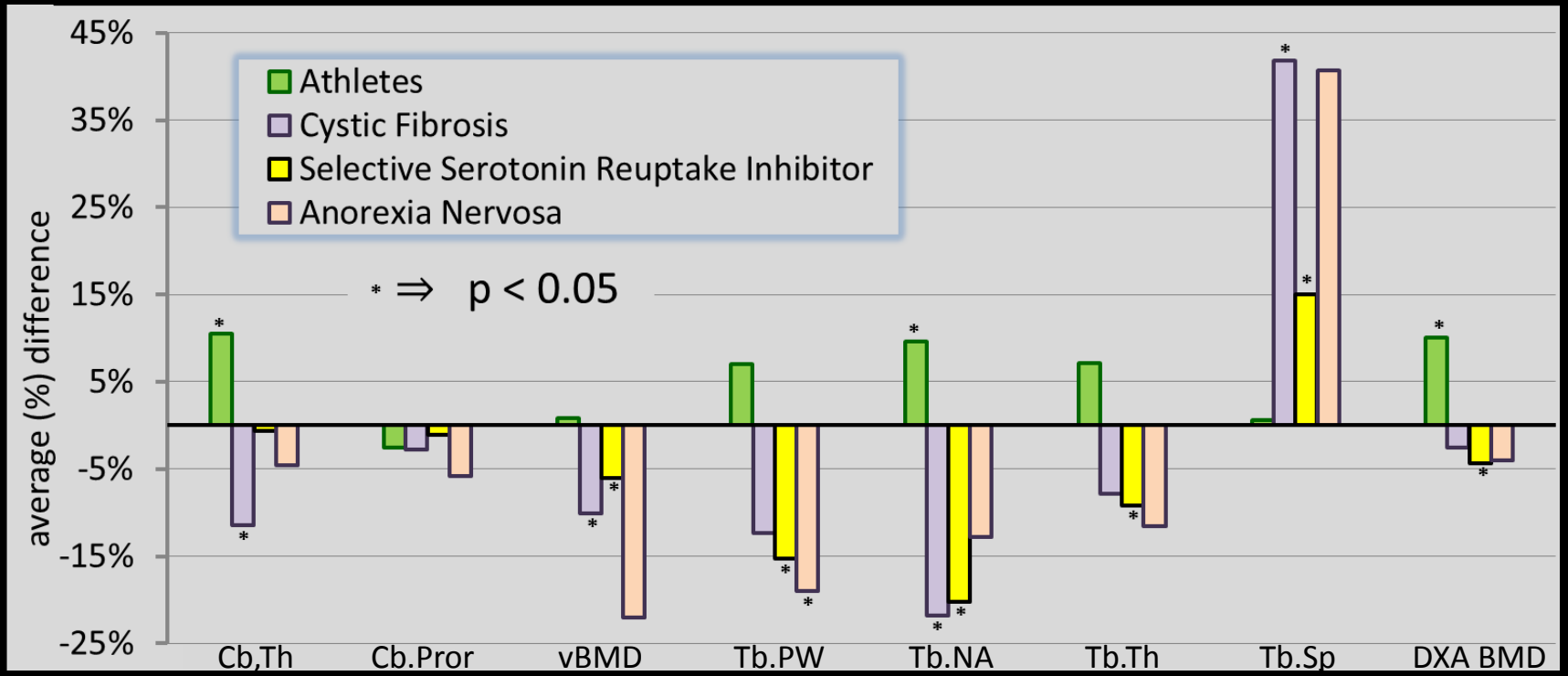

Average differences of bone measures in athlete (N=10), cystic fibrosis (N=11), selective serotonin reuptake inhibitor (N=12), and anorexia nervosa (N=4) groups as compared to age-sex-BMI-similar healthy controls from the Iowa Bone Development Study (N=102). Age-sex-height matching was used for the anorexia nervosa group.

Bone Characterization in Different Patient Groups

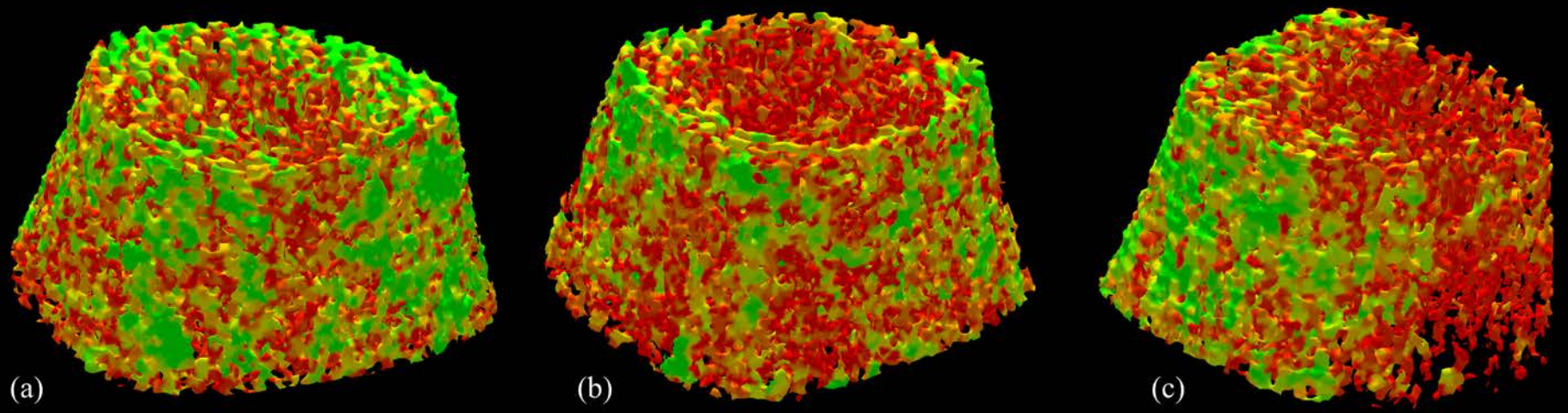

Color-coded illustration of trabecular bone (TB) plate/rod classification for a IBDS female control (a) and an age-similar, sex- and BMI-matched patient on continuous treatment with an SSRI (b), and another age-similar, sex- and BMI-matched patient with confirmed diagnosis of CF (c). The healthy female (a) has more TB plates (green) as compared to the two patient participants. Between the two patients, the CF patient (c) has some signs of heterogeneous bone loss.

Study 3

Aim: To determine bone structural differences in fracture vs non0-fracture groups

Bone Structural Differences in vertebral Fracture vs Non-Fracture Groups

- 30 patients (13 male) with COPD GOLD status between 1 and 4
- age: 70.6±8.1 years BMI: 27.5±4.2
- 23 patients with at one vertebral fracture

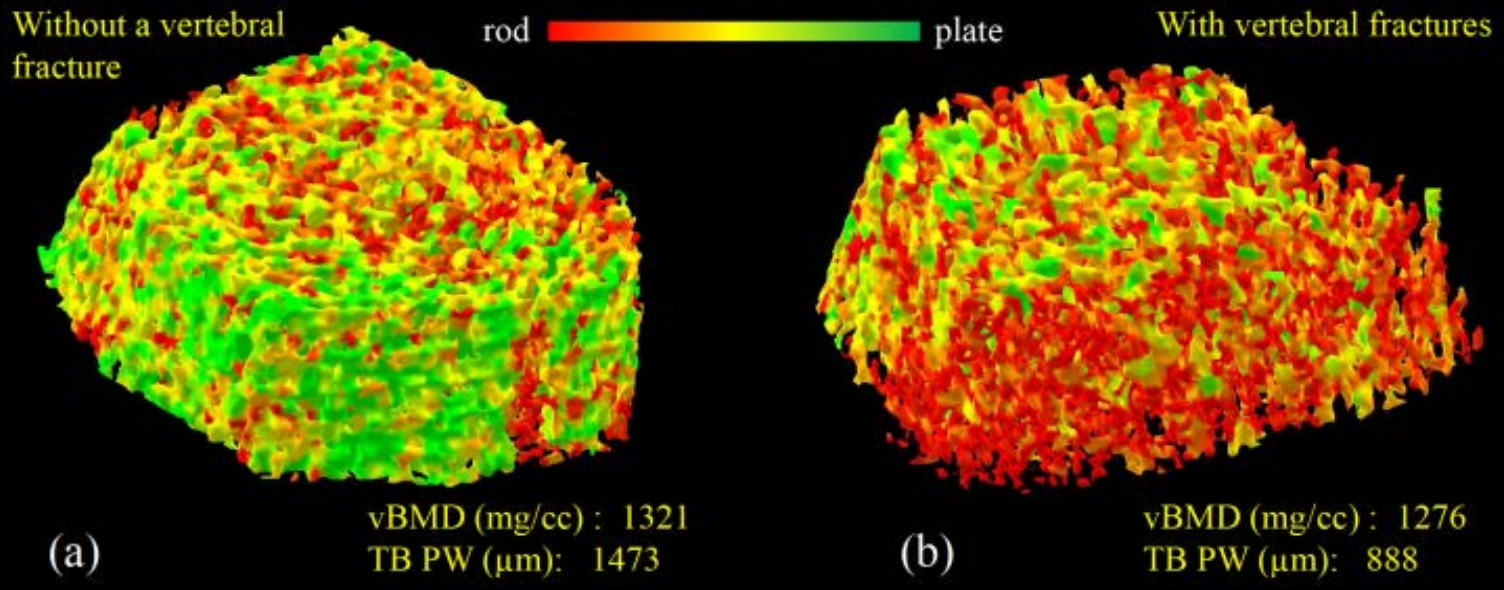

- The patient without a vertebral fracture has ≈ 50% more Tb plates (green)
- The difference in Tb volumetric BMD between the two male patients is only 3.5%

Bone Structural Differences in vertebral Fracture vs Non-Fracture Groups

- 30 patients (13 male) with COPD GOLD status between 1 and 4
- age: 70.6±8.1 years BMI: 27.5±4.2
- 23 patients with at one vertebral fracture

	CB Th (μm)	CB Poro	v-BMD (mg/cc)	pBMD (mg/cc)	tBMD (mg/cc)	TB NA (mm^2/mm^3)	TB PW (μm)	TB Th (μm)	TB Sp (μm)
Non-fracture	1862	0.20	1101	818	222	0.47	995.0	120.5	513.5
Fracture	1745	0.21	1088	723	181	0.41	889.3	121.6	571.6
Difference	6.3%	-6.4%	1.2%	11.6%	18.3%	13.6%	10.6%	-0.9%	-11.3%
p-value	0.328	0.226	0.147	0.056	0.054	0.058	0.090	0.427	0.279

The difference (%) in MDCT-based bone measures between fracture (n = 23) and non-fracture (n = 7) groups of patients with COPD

Study 4

Aim: To determine the normative distribution of MDCT bone measures and their relationships with DXA

Normative Distribution of MDCT Bone Measures and their Relationships with DXA

- Healthy volunteers (N = 324) from the Iowa Bone Development Study
- Age: 19.8 ± 0.7 years
- 178 females and 146 males
- Cb measures were computed over 14-16% of tibia, while Tb measures were computed over 4-6% of tibia with a 30% peel (Table 1)
- Whole-body, hip, spine, and left-leg DXA areal BMD measures were obtained on a Hologic Discovery A model densitometer

Normative Distribution of Bone Measures

Variables	*Males (n=146)*	*Females (n = 178)*
Scan-age (Y)	19.77 (0.74)	19.77 (0.69)
Height (cm)	180.2 (7.7)**	166.4 (6.9)
Weight (kg)	84.74 (19.90)**	70.64 (19.31)
BMI	26.05 (5.60)	25.44 (6.49)
DXA aBMD		
Whole-body	1.283 (0.099)**	1.165 (0.090)
Hip	1.174 (0.165)**	1.031 (0.132)
Spine	1.099 (0.119)**	1.054 (0.130)
Left leg	1.390 (0.125)**	1.205 (0.103)
MDCT Cortical		
Cb.poro	0.219 (0.022)**	0.205 (0.042)
Cb.Th (mm)	2.319 (0.269)**	2.006 (0.236)
MDCT Trabecular		
Tb.vBMD (mg/cc)	1182.9 (27.7)**	1164.4 (32.1)
Tb.tBMD (mg/cc)	360.4 (74.2)**	312.1 (86.3)
Tb.pBMD (mg/cc)	1005.0 (103.1)**	928.2 (120.9)
Tb.NA (mm^2/mm^3)	0.063 (0.013)**	0.050 (0.013)
Tb.PW (μm)	1375.7 (300.2)**	1211.0 (315.9)
Tb.Th (μm)	173.2 (24.9)**	161.6 (23.8)
Tb.Sp (μm)	398.0 (63.9)**	439.6 (85.1)

Correlations for MDCT Cortical and Trabecular Bone Outcomes with DXA Areal BMD

Female									
Variable	*Cb.poro*	*Cb.Th*	*Tb.vBMD*	*Tb.tBMD*	*Tb.pBMD*	*Tb.NA*	*Tb.PW*	*Tb.Th*	*Tb.Sp*
Whole-body	-0.08	0.39**	0.64**	0.61**	0.58**	0.64**	0.61**	0.53**	-0.57**
Hip	-0.06	0.44**	0.61**	0.60**	0.56**	0.63**	0.58**	0.50**	-0.54**
Spline	-0.08	0.29**	0.49**	0.46**	0.40**	0.46**	0.44**	0.36**	-0.43**
Left leg	-0.07	0.60**	0.64**	0.65**	0.64**	0.69**	0.65**	0.61**	-0.57**

Male									
Variable	*Cb.poro*	*Cb.Th*	*Tb.vBMD*	*Tb.tBMD*	*Tb.pBMD*	*Tb.NA*	*Tb.PW*	*Tb.Th*	*Tb.Sp*
Whole-body	0.20*	0.41**	0.48**	0.48**	0.41**	0.55**	0.40**	0.36**	-0.50**
Hip	0.08	0.41**	0.55**	0.54**	0.48**	0.59**	0.48**	0.43**	-0.53**
Spline	0.17*	0.29**	0.34**	0.34**	0.30**	0.37**	0.26**	0.25**	-0.34**
Left leg	0.18*	0.51**	0.57**	0.54**	0.52**	0.61**	0.52**	0.50**	-0.52**

Moderate correlations between MDCT and DXA outcomes suggest uniqueness of bone structural properties captured by MDCT measures as compared to DXA

Conclusions

- Advanced quantitative characterization of bone micro-architecture are suited for medical imaging research and clinical studies.
- Multi-detector CT is a potential imaging modality for *in vivo* assessment of human trabecular bone micro-architecture
- Bone data from multiple MDCT scanners can be used in large studies after adjustment using proper calibration equation
- Normative distributions of MDCT bone measures are define disease groups
- Low to moderate correlation for MDCT bone measures with DXA outcomes suggests uniqueness of MDCT measures
- Bone structural differences in different human groups may provide new insights of the etiology of bone diseases
- MDCT bone measures may be useful to predict fracture risk

References

[1] JM Abrahams, PK Saha, RW Hurst, PD LeRous, and JK Udupa, "Three dimensional bone-free rendering of the crebral circulation using computed tomographic angiography and fuzzy connectedness," *Neurosurgery*, **51**, 264-269, 2002.

[2] G Chang, SK Pakin, ME Schweitzer, PK Saha, and RR Regatte, "Adaptations in trabecular bone microarchitecture in Olympic athletes determined by 7T MRI," *J Magn Reson Imaging*, **27**, 1089-95, 2008, PubMed Central PMCID: PMCPMC3850284.

[3] G Chang, D Xia, C Chen, G Madelin, SB Abramson, JS Babb, PK Saha, and RR Regatte, "7T MRI detects deterioration in subchondral bone microarchitecture in subjects with mild knee osteoarthritis as compared with healthy controls," *Journal of Magnetic Resonance Imaging*, **41**, 1311-1317, 2015.

[4] C Chen, D Jin, Y Liu, FW Wehrli, G Chang, PJ Snyder, RR Regatte, and PK Saha, "Trabecular bone characterization on the continuum of plates and rods using in vivo MR imaging and volumetric topological analysis," *Physics in Medicine and Biology*, **61**, N478-N496, 2016.

[5] KC Ciesielski, JK Udupa, PK Saha, and Y Zhuge, "Iterative relative fuzzy connectedness for multiple objects with multiple seeds," *Computer Vision and Image Understanding*, **107**, 160-182, 2007.

[6] KC Ciesielski, R Strand, F Malmberg, and PK Saha, "Efficient algorithm for finding the exact minimum barrier distance," *Computer Vision and Image Understanding*, **123**, 53-64, 2014.

[7] S Dudley-Javoroski, PK Saha, G Liang, C Li, Z Gao, and RK Shields, "High dose compressive loads attenuate bone mineral loss in humans with spinal cord injury," *Osteoporosis International*, **23**, 2335-2346, 2012, PubMed Central PMCID: PMC3374128.

[8] S Dudley-Javoroski, R Amelon, YX Liu, PK Saha, and RK Shields, "High bone density masks architectural deficiencies in an individual with spinal cord injury," *Journal of Spinal Cord Medicine*, **37**, 349-354, 2014, PubMed Central PMCID: PMC4064585.

References .....*Continued*

[9] S Dudley-Javoroski, MA Petrie, CL McHenry, RE Amelon, PK Saha, and RK Shields, "Bone architecture adaptations after spinal cord injury: impact of long-term vibration of a constrained lower limb," *Osteoporosis International*, 1-12, 2015.

[10] S Dudley-Javoroski, M Petrie, C McHenry, R Amelon, P Saha, and R Shields, "Bone architecture adaptations after spinal cord injury: impact of long-term vibration of a constrained lower limb," *Osteoporosis International*, **27**, 1149-1160, 2016.

[11] Z Gao, R Grout, C Holtze, EA Hoffman, and PK Saha, "A new paradigm of interactive artery/vein separation in non-contrast pulmonary CT imaging using multi-scale topo-morphologic opening," *IEEE Trans Biomed Eng*, **59**, 3016-3027, 2012.

[12] BR Gomberg, PK Saha, HK Song, SN Hwang, and FW Wehrli, "Topological analysis of trabecular bone MR images," *IEEE Transactions on Medical Imaging*, **19**, 166-174, 2000.

[13] BR Gomberg, FW Wehrli, B Vasilic, RH Weening, PK Saha, HK Song, and AC Wright, "Reproducibility and error sources of micro-MRI-based trabecular bone structural parameters of the distal radius and tibia," *Bone*, **35**, 266-76, 2004.

[14] BR Gomberg, PK Saha, and FW Wehrli, "Method for cortical bone structural analysis from magnetic resonance images," *Academic Radiology*, **12**, 1320-1332, 2005.

[15] LM Griffin, S Honig, C Chen, PK Saha, R Regatte, and G Chang, "7T MRI of distal radius trabecular bone microarchitecture: How trabecular bone quality varies depending on distance from end-of-bone," *Journal of Magnetic Resonance Imaging*, 2016.

[16] A Hotca, CS Rajapakse, C Cheng, S Honig, K Egol, RR Regatte, PK Saha, and G Chang, "In vivo measurement reproducibility of femoral neck microarchitectural parameters derived from 3T MR images," *Journal of Magnetic Resonance Imaging*, 2015.

References .....*Continued*

[17] KS Iyer, JD Newell Jr, D Jin, MK Fuld, PK Saha, S Hansdottir, and EA Hoffman, "Quantitative dual-energy computed tomography supports a vascular etiology of smoking-induced inflammatory lung disease," *American journal of respiratory and critical care medicine*, **193**, 652-661, 2016.

[18] D Jin and PK Saha, "A new fuzzy skeletonization algorithm and its applications to medical imaging," Proc. of *17th Int Conf Imag Anal Proc (ICIAP)*, **LNCS 8156**, 662-671, Naples, Italy, September 11-13 2013.

[19] D Jin, Y Liu, and PK Saha, "Application of fuzzy skeletonization to quantitative assess of trabecular bone micro-architecture," Proc. of *35th International Conference of the IEEE Engineering in Medicine and Biology Society,* Osaka, Japan, July 3-7 2013.

[20] D Jin, KS Iyer, EA Hoffman, and PK Saha, "A New Approach of Arc Skeletonization for Tree-Like Objects Using Minimum Cost Path," Proc. of *22nd International Conference on Pattern Recognition*, 942-947, Stockholm, Sweden, 24-28 August 2014.

[21] D Jin, KS Iyer, EA Hoffman, and PK Saha, "Automated assessment of pulmonary arterial morphology in multi-row detector CT imaging using correspondence with anatomic airway branches," Proc. of *International Symposium on Visual Computing (ISVC)*, **LNCS 8887**, 521-530, Las Vegas, NV, December 8-10 2014.

[22] D Jin, C Chen, and PK Saha, "Filtering non-significant quench points using collision impact in grassfire propagation," Proc. of *18th Int Conf Imag Anal Proc (ICIAP)*, **9279** 432-443, Genoa, Italy, September 9-11 2015.

[23] D Jin, KS Iyer, C Chen, EA Hoffman, and PK Saha, "A robust and efficient curve skeletonization algorithm for tree-like objects using minimum cost paths," *Pattern Recognition Letters*, **76**, 32-40, 2016.

[24] CE Jones, RL Wolf, JA Detre, B Das, PK Saha, J Wang, Y Zhang, HK Song, AC Wright, ER Mohler, RM Fairman, EL Zager, OC Velazquez, MA Golden, JP Carpenter, and FW Wehrli, "Structural MRI of carotid artery atherosclerotic lesion burden and characterization of hemispheric cerebral blood flow before and after carotid endarterectomy," *NMR in Biomedicine*, **19**, 198-208, 2006.

References .....*Continued*

[25] TY Kong, PK Saha, and A Rosenfeld, "Strongly normal sets of tiles in n-dimensions," *Pattern Recognition*, **40**, 530-543, 2007.

[26] GA Ladinsky, B Vasilic, A Popescu, M Wald, B Zemel, PJ Snyder, L Loh, HK Song, PK Saha, AC Wright, and FW Wehrli, "Trabecular structure correlates of vertebral deformity by micro-MRI," Proc. of *Bone quality: What is it and Can We Measure it?*, 27, Bethesda, 2005.

[27] GA Ladinsky, B Vasilic, A Popescu, M Wald, B Zemel, PJ Snyder, L Loh, HK Song, PK Saha, AC Wright, and FW Wehrli, "Degree of Vertebral Deformities is Associated with Topology of Trabecular Network Measured Noninvasively at Radius and Tibia Surrogate Sites," Proc. of *ASBMR, 27th Annual Meeting*, **in press**, S383, Nashville, 2005.

[28] GA Ladinsky, B Vasilic , AM Popescu, B Zemel, AC Wright, HK Song, PK Saha, H Peachy, PK Snyder, and FW Wehrli, "MRI Based Virtual Bone Biopsy Detects Large One-Year Changes in Trabecular Bone Architecture of Early Postmenopausal Women," Proc. of *ASBMR, 27th Annual Meeting*, S15, Nashville, 2005.

[29] GA Ladinsky, B Vasilic, AM Popescu, M Wald, BS Zemel, PJ Snyder, L Loh, HK Song, PK Saha, AC Wright, and FW Wehrli, "Trabecular structure quantified with the MRI-based virtual bone biopsy in postmenopausal women contributes to vertebral deformity burden independent of areal vertebral BMD," *J Bone Miner Res*, **23**, 64-74, 2008, PubMed Central PMCID: PMC2663589.

[30] SC Lam, MJ Wald, CS Rajapakse, Y Liu, PK Saha, and FW Wehrli, "Performance of the MRI-based virtual bone biopsy in the distal radius: serial reproducibility and reliability of structural and mechanical parameters in women representative of osteoporosis study populations," *Bone*, **49**, 895-903, 2011, PubMed Central PMCID: PMC3167016.

[31] T Lei, JK Udupa, PK Saha, and D Odhner, "Artery-vein separation via MRA - an image processing approach," *IEEE Transactions on Medical Imaging*, **20**, 689-703, 2001.

References .....*Continued*

[32] T Lei, JK Udupa, PK Saha, D Odhner, R Baum, ST Tadikonda, and EK Yucel, "3D MRA visualization and Artery-Vein Separation using blood-pool contrast agent MS-325," *Academic Radiology*, **9**, S127-S133, 2002.

[33] C Li, D Jin, C Chen, EM Letuchy, KF Janz, TL Burns, JC Torner, SM Levy, and PK Saha, "Automated cortical bone segmentation for multirow-detector CT imaging with validation and application to human studies," *Med Phys*, **42**, 4553-65, 2015, PubMed Central PMCID: PMC4499051.

[34] XS Liu, P Sajda, PK Saha, FW Wehrli, and XE Guo, "Quantification of the roles of trabecular microarchitecture and trabecular type in determining the elastic modulus of human trabecular bone," *J Bone Miner Res*, **21**, 1608-1617, 2006.

[35] XS Liu, P Sajda, PK Saha, FW Wehrli, G Bevill, TM Keaveny, and XE Guo, "Complete volumetric decomposition of individual trabecular plates and rods and its morphological correlations with anisotropic elastic moduli in human trabecular bone," *J Bone Miner Res*, **23**, 223-35, 2008, PubMed Central PMCID: PMC2665696.

[36] Y Liu, PK Saha, and Z Xu, "Quantitative characterization of trabecular bone micro-architecture using tensor scale and multi-detector CT imaging," Proc. of *Med Image Comput Comput Assist Interv*, **15**, 124-131, 2012.

[37] Y Liu, G Liang, and PK Saha, "A new multi-object image thresholding method based on correlation between object class uncertainty and intensity gradient," *Med Phys*, **39**, 514-32, 2012, PubMed Central PMCID: PMC3266827.

[38] Y Liu, D Jin, C Li, KF Janz, TL Burns, JC Torner, SM Levy, and PK Saha, "A robust algorithm for thickness computation at low resolution and its application to in vivo trabecular bone CT imaging," *IEEE Transactions on Biomedical Engineering*, **61**, 2057-2069, 2014, PubMed Central PMCID: PMCNIHMSID696943.

[39] L Nyúl, JK Udupa, and PK Saha, "Incorporating a measure of local scale in voxel-based 3D image registration," *IEEE Transactions on Medical Imaging*, **22**, 228-237, 2003.

[40] PK Saha, B Chanda, and DD Majumder, "Principles and algorithms for 2-D and 3-D shrinking," Indian Statistical Institute, Calcutta, India, TR/KBCS/2/91, 1991.

References .....*Continued*

[41] PK Saha and BB Chaudhuri, "Simple point computation and 3-D thinning with parallel implementation," Indian Statistical Institute, Calcutta, India, TR/KBCS/1/93, 1993.

[42] PK Saha and BB Chaudhuri, "Detection of 3-D simple points for topology preserving transformations with application to thinning," *IEEE Transactions on Pattern Analysis and Machine Intelligence*, **16**, 1028-1032, 1994.

[43] PK Saha, BB Chaudhuri, B Chanda, and DD Majumder, "Topology preservation in 3D digital space," *Pattern Recognition*, **27**, 295-300, 1994.

[44] PK Saha and BB Chaudhuri, "3D digital topology under binary transformation with applications," *Computer Vision and Image Understanding*, **63**, 418-429, 1996.

[45] PK Saha, BB Chaudhuri, and DD Majumder, "A new shape preserving parallel thinning algorithm for 3D digital images," *Pattern Recognition*, **30**, 1939-1955, 1997.

[46] PK Saha, DD Majumder, and A Rosenfeld, "Local topological parameters in a tetrahedral representation," *Graphical Models Image Processing*, **60**, 423-436, 1998.

[47] PK Saha and A Rosenfeld, "Strongly normal sets of convex polygons or polyhedra," *Pattern Recognition Letters*, **19**, 1119-1124, 1998.

[48] PK Saha, BR Gomberg, and FW Wehrli, "Three-dimensional digital topological characterization of cancellous bone architecture," *International Journal of Imaging Systems and Technology*, **11**, 81-90, 2000.

[49] PK Saha and JK Udupa, "Iterative relative fuzzy connectedness and object definition: theory, algorithms, and applications in image segmentation," Proc. of *IEEE Workshop on Mathematical Methods in Biomedical Image Analysis*, Hilton Head, South Carolina, 2000.

[50] PK Saha, JK Udupa, and D Odhner, "Scale-based fuzzy connected image segmentation: theory, algorithms, and validation," *Computer Vision and Image Understanding*, **77**, 145-174, 2000.

References .....*Continued*

[51] PK Saha and A Rosenfeld, "The digital topology of sets of convex voxels," *Graphical Models Image Processing*, **62**, 343-352, 2000.

[52] PK Saha and A Rosenfeld, "Determining simplicity and computing topological change in strongly normal partial tilings of R^2 or R^3," *Pattern Recognition*, **33**, 105-118, 2000.

[53] PK Saha and JK Udupa, "Relative fuzzy connectedness among multiple objects: theory, algorithms, and applications in image segmentation," *Computer Vision and Image Understanding*, **82**, 42-56, 2001.

[54] PK Saha and JK Udupa, "Fuzzy connected object delineation: axiomatic path strength definition and the case of multiple seeds," *Computer Vision and Image Understanding*, **83**, 275-295, 2001.

[55] PK Saha and JK Udupa, "Scale based image filtering preserving boundary sharpness and fine structures," *IEEE Transactions on Medical Imaging*, **20**, 1140-1155, 2001.

[56] PK Saha and A Rosenfeld, "Local and global topology preservation in locally finite sets of tiles," *Information Sciences*, **137**, 303-311, 2001.

[57] PK Saha and JK Udupa, "Optimum threshold selection using class uncertainty and region homogeneity," *IEEE Transactions on Pattern Analysis and Machine Intelligence*, **23**, 689-706, 2001.

[58] PK Saha, JK Udupa, EF Conant, DP Chakraborty, and D Sullivan, "Breast tissue glandularity quantification via digitized mammograms," *IEEE Transactions on Medical Imaging*, **20**, 792-803, 2001.

[59] PK Saha, FW Wehrli, and BR Gomberg, "Fuzzy distance transform: theory, algorithms, and applications," *Computer Vision and Image Understanding*, **86**, 171-190, 2002.

[60] PK Saha and FW Wehrli, "Fuzzy distance transform in general digital grids and its applications," Proc. of *7th Joint Conference on Information Sciences*, 201-213, Research Triangular Park, NC, 2003.

[61] PK Saha and FW Wehrli, "Measurement of trabecular bone thickness in the limited resolution regime of in vivo MRI by fuzzy distance transform," *IEEE Trans Med Imaging*, **23**, 53-62, 2004.

References .....*Continued*

[62] PK Saha and FW Wehrli, "A robust method for measuring trabecular bone orientation anisotropy at in vivo resolution using tensor scale," *Pattern Recognition*, **37**, 1935-1944, 2004.

[63] PK Saha, JK Udupa, AX Falcão, BE Hirsch, and S Siegler, "Iso-shaping rigid bodies for estimating their motion from image sequences," *IEEE Transactions on Medical Imaging*, **23**, 63-72, 2004.

[64] PK Saha, "Tensor scale: a local morphometric parameter with applications to computer vision and image processing," *Computer Vision and Image Understanding*, **99**, 384-413, 2005.

[65] PK Saha, B Das, and FW Wehrli, "An object class-uncertainty induced adaptive force and its application to a new hybrid snake," *Pattern Recognition*, **40**, 2656-2671, 2007.

[66] PK Saha, Z Gao, SK Alford, M Sonka, and EA Hoffman, "Topomorphologic separation of fused isointensity objects via multiscale opening: separating arteries and veins in 3-D pulmonary CT," *IEEE Transactions on Medical Imaging*, **29**, 840-851, 2010.

[67] PK Saha, Y Xu, H Duan, A Heiner, and G Liang, "Volumetric topological analysis: a novel approach for trabecular bone classification on the continuum between plates and rods," *IEEE Trans Med Imaging*, **29**, 1821-38, 2010, PubMed Central PMCID: PMC3113685.

[68] PK Saha, G Liang, JM Elkins, A Coimbra, LT Duong, DS Williams, and M Sonka, "A new osteophyte segmentation algorithm using partial shape model and its applications to rabbit femur anterior cruciate ligament transection via micro-CT imaging," *IEEE Transactions on Biomedical Engineering*, **58**, 2212-2227, 2011.

[69] PK Saha, R Strand, and G Borgefors, "Digital Topology and Geometry in Medical Imaging: A Survey," *IEEE Trans Med Imaging*, **34**, 1940-64, 2015.

[70] PK Saha, Y Liu, C Chen, D Jin, EM Letuchy, Z Xu, RE Amelon, TL Burns, JC Torner, SM Levy, and CA Calarge, "Characterization of trabecular bone plate-rod microarchitecture using multirow detector CT and the tensor scale: Algorithms, validation, and applications to pilot human studies," *Med Phys*, **42**, 5410-5425, 2015, PubMed Central PMCID: PMC4545095.

References .....*Continued*

[71] PK Saha, G Borgefors, and G Sanniti di Baja, "A survey on skeletonization algorithms and their applications," *Pattern Recognition Letters*, **76**, 3-12, 2016.

[72] PK Saha, G Borgefors, and G Sanniti di Baja, "Skeletonization and its applications-a review," in *Skeletonization: Theory Methods, and Applications*, P. K. Saha, G. Borgefors, and G. Sanniti di Baja, Eds., Academic Press, 2017.

[73] PK Saha, G Borgefors, and G Sanniti di Baja, *Skeletonization: Theory, Methods, and Applications*, Academic Press, 2017.

[74] PK Saha, D Jin, Y Liu, GE Christensen, and C Chen, "Fuzzy object skeletonization: theory, algorithms, and applications," *IEEE Transactions on Visualization and Computer Graphics*, in press.

[75] N Sladoje, I Nyström, and PK Saha, "Measurements of digitized objects with fuzzy borders in 2D and 3D," *Image and Vision Computing*, **23**, 123-132, 2005.

[76] R Strand, KC Ciesielski, F Malmberg, and PK Saha, "The minimum barrier distance," *Computer Vision and Image Understanding*, **117**, 429-437, 2013.

[77] JK Udupa, PK Saha, and RA Lotufo, "Relative fuzzy connectedness and object definition: theory, algorithms, and applications in image segmentation," *IEEE Transactions on Pattern Analysis and Machine Intelligence*, **24**, 1485-1500, 2002.

[78] JK Udupa and PK Saha, "Fuzzy connectedness and image segmentation," *Proceedings of the IEEE*, **91**, 1649-1669, 2003.

[79] DM Vasilescu, Z Gao, PK Saha, L Yin, G Wang, B Haefeli-Bleuer, M Ochs, ER Weibel, and EA Hoffman, "Assessment of morphometry of pulmonary acini in mouse lungs by nondestructive imaging using multiscale microcomputed tomography," *Proc Natl Acad Sci U S A*, **109**, 17105-10, 2012, PubMed Central PMCID: PMC3479519.

[80] MJ Wald, B Vasilic, PK Saha, and FW Wehrli, "Spatial autocorrelation and mean intercept length analysis of trabecular bone anisotropy applied to in vivo magnetic resonance imaging," *Med Phys*, **34**, 1110-20, 2007.

References .....*Continued*

[81] FW Wehrli, PK Saha, and BR Gomberg, "Digital topological analysis of trabecular bone MR images and prediction of osteoporosis fractures," *U.S. Application filed by the University of Pennsylvania*, **Penn Docket N2493**, 2000.

[82] FW Wehrli, BR Gomberg, PK Saha, HK Song, SN Hwang, and PJ Snyder, "Digital topological analysis of in vivo magnetic resonance microimages of trabecular bone reveals structural implications of osteoporosis," *Journal of Bone Mineral Research*, **16**, 1520-1531, 2001.

[83] FW Wehrli, PK Saha, BR Gomberg, HK Song, PJ Snyder, M Benito, A Wright, and R Weening, "Role of magnetic resonance for assessing structure and function of trabecular bone," *Top Magn Reson Imaging*, **13**, 335-55, 2002.

[84] FW Wehrli, PK Saha, BR Gomberg, and HK Song, "Noninvasive assessment of bone architecture by magnetic resonance micro-imaging-based virtual bone biopsy," *Proceedings of IEEE, Emerging Medical Imaging Technology, (invited paper)*, **91**, 1520-1542, 2003.

[85] FW Wehrli, MB Leonard, PK Saha, and BG Gomberg, "Quantitative high-resolution MRI reveals structural implications of renal osteodystrophy on trabecular and cortical bone," *J Magn Reson Imaging*, **20**, 83-89, 2004.

[86] FW Wehrli and PK Saha, "Quantification of 3D Topology and Scale of Trabecular Bone in the Limited Spatial Resolution Regime of in Vivo Micro-MRI," *Microscopy and Microanalysis*, **10**, 718-719, 2004.

[87] FW Wehrli, HK Song, PK Saha, and AC Wright, "Quantitative MRI for the assessment of bone structure and function," *NMR Biomed*, **19**, 731-64, 2006.

[88] FW Wehrli, GA Ladinsky, C Jones, M Benito, J Magland, B Vasilic, AM Popescu, B Zemel, AJ Cucchiara, AC Wright, HK Song, PK Saha, H Peachey, and PJ Snyder, "In vivo magnetic resonance detects rapid remodeling changes in the topology of the trabecular bone network after menopause and the protective effect of estradiol," *J Bone Miner Res*, **23**, 730-40, 2008, PubMed Central PMCID: PMC2674544.

[89] Z Xu, M Sonka, and PK Saha, "Improved tensor scale computation with application to medical image interpolation," *Comput Med Imaging Graph*, **35**, 64-80, 2011.

References .....*Continued*

[90] Y Xu, G Liang, G Hu, Y Yang, J Geng, and PK Saha, "Quantification of coronary arterial stenoses in CTA using fuzzy distance transform," *Computerized Medical Imaging and Graphics*, **36**, 11-24, 2012.

[91] Z Xu, PK Saha, and S Dasgupta, "Tensor scale: An analytic approach with efficient computation and applications," *Comput Vis Image Underst*, **116**, 1060-1075, 2012, PubMed Central PMCID: PMC4519998.

[92] Y Zhuge, JK Udupa, and PK Saha, "Vectorial scale-based fuzzy connected image segmentation," *Computer Vision and Image Understanding*, **101**, 177-193, 2006.

Acknowledgments

Collaborators

Steven M. Levy, Eric Hoffman, Trudy L. Burns, Richard Shields, Chadi A. Calarge, James C. Torner, Laurie M. McCormick, Ravi Regatte, X. Edward Guo, Felix W. Wehrli, Elizabeth Regan, Alexadro Comellas

Scientists/Post-doctoral Fellows/Engineers

Guoyuan Liang, Duan Hong, Subhadip Basu, Jamuna Kanta Singh, Ryan Amelon, Zhiyun Gao

Graduate Students

Zhiyun Gao, Yinxiao Liu, Ziyue Xu, Yan Xu, Cheng Li Dakai Jin, Cheng Chen, Xiaoliu Zhang, Syed Nadeem Ahmed, Indranil Guha

Grant Acknowledgments

- NIH R01 AR054439 (PI: Saha)
- ICTS/CTSA pilot grant (PI: Saha)
- NIH R01 AR051376 (Sub-contract PI: Saha; Columbia University)
- NIH R01 AR056260 (Sub-contract PI: Saha; New York University)
- NIH R01 DE012101-13S1 (PI: Levy)
- NIH R01 HD062507 (PI: Shields)
- NIH R01 HL-064368 (PI: Hoffman)

THANK YOU!